UNIVERSITY OF CALIFORNIA, SAN DIEGO

Energy Storage Systems for High PV Penetration: Utility Spatial Allocation and Customer Dispatch Strategies

A dissertation submitted in partial satisfaction of the
requirements for the degree Doctor of Philosophy

in

Engineering Sciences (Mechanical Engineering)

by

Oytun Babacan

Committee in charge:

Jan Kleissl, Chair
Richard T. Carson
Carlos F.M. Coimbra
William V. Torre
George R. Tynan
David G. Victor

2017

The Dissertation of Oytun Babacan is approved and is acceptable in quality and form for publication on microfilm and electronically:

_____

_____

_____

_____

_____

_____

Chair

University of California, San Diego

2017

DEDICATION

To my parents and my brother.

TABLE OF CONTENTS

LIST OF FIGURES

LIST OF TABLES

ACKNOWLEDGEMENTS

I would like to acknowledge all the support that I have received throughout my graduate studies from my family and my friends. Without their constant support, especially from my parents and my brother, it would be impossible to do all the hard work which has led to this dissertation.

I gratefully acknowledge the mentorship of my advisor Professor Jan Kleissl. Through his guidance I have found the balance between abstraction and application. And, William Torre whose support inspired me to pursue the work in this dissertation. I am thankful to my committee members, Professor David Victor, Professor George Tynan, Professor Carlos Coimbra, and Professor Richard Carson, for their valuable comments and suggestions during the preparation of this dissertation.

I acknowledge the support of all my colleagues and collaborators at the University of California, San Diego. I am thankful to my colleagues Ryan Hanna, Mohamed Ghonima, Ryan Hanna, Elizabeth Ratnam, Vahid Disfani, Ahmed Abdulla, Handa Yang, Andu Nyugen, and Ben Kurtz. I enjoyed the company of all members of the Solar Resource Assessment and Forecasting Laboratory, who were part of a unique environment for sharing knowledge and curiosity.

The friendships I had here in San Diego made this beautiful sunny place a second home to me. If I had a chance to live through these years again I would only wish to have the same truly amazing experience. I was very lucky to know Amedeo, Mohamed, Ryan, Marine, Marta, Augusta, George, Jesus (Bueno), Kristen, Marghe, Sandra, Handa, Andrei, Costas, who showed me the good ways to live a life. I hope to have many other moments with all the beautiful people I met here.

The text and data in Chapter 1, in full, is a reprint of the material as it appears in "Siting and sizing of distributed energy storage to mitigate voltage impact by solar PV in distribution systems", Babacan, Oytun; Torre, William, Kleissl, Jan, *Solar Energy*, 146

(2017), 199-208. The dissertation author is the primary investigator and author of this article.

The text and data in Chapter 2, in full, is submitted for publication of the material with the title “Distributed energy storage system scheduling considering tariff structure, energy arbitrage and solar PV penetration”. Babacan, Oytun; Ratnam, Elizabeth L.; Disfani, Vahid R.; Kleissl, Jan. The dissertation author is the primary investigator and author of this article.

Chapter 3, in part, is currently being prepared for submission for publication of material. Babacan, Oytun; Hanna, Ryan; Abdulla, Ahmed; Kleissl, Jan; Victor, David. The dissertation author is the primary investigator and author of this article.

VITA

2010	Bachelor of Science, Boğaziçi Üniversitesi, Turkey
2012	Master of Science, University of Illinois Urbana-Champaign
2017	Doctor of Philosophy, University of California San Diego

PUBLICATIONS

O. Babacan; R. Hanna, A. Abdulla, J. Kleissl and D. Victor. "Emissions impact of residential battery energy storage: Would the adoption of residential energy storage in the U.S. be effective in reducing emissions?". In: Preparation.

O. Babacan; E. Ratnam, V. Disfani and J. Kleissl. "Distributed energy storage system scheduling considering tariff structure, energy arbitrage and solar PV penetration". In: Review.

J. Bright; **O. Babacan**; J. Kleissl; P.G. Taylor and R. Crook. "A synthetic, spatially decorrelating solar irradiance generator and application to a LV grid model with high PV penetration". In: Solar Energy 147 (2017), pp. 83 - 98.

O. Babacan; W. Torre and J. Kleissl. "Siting and sizing of distributed energy storage to mitigate voltage impact by solar PV in distribution systems". In: Solar Energy 146 (2017), pp. 199 - 208.

O. Babacan; W. Torre and J. Kleissl. "Optimal Allocation of Battery Energy Storage Systems in Distribution Networks Considering High PV Penetration". In: Power and Energy Society General Meeting (PESGM). Boston, MA, July 2016.

ABSTRACT OF THE DISSERTATION

Energy Storage Systems for High PV Penetration: Utility Spatial Allocation and Customer Dispatch Strategies

by

Oytun Babacan

Doctor of Philosophy in Engineering Sciences (Mechanical Engineering)

University of California, San Diego, 2017

Jan Kleissl, Chair

Climate change mitigation motivates the transformation of the electric power sector towards a low carbon future. A successful and timely transformation depends on robust and independent methods for understanding benefits and impacts of the integration of renewable energy resources and energy storage technologies into the electric power system. Therefore the objectives of this dissertation are to investigate how energy storage technologies should be allocated and operated to mitigate the impacts of variable solar photovoltaic (PV) resources in distribution systems while providing economic incentives for storage owners, and to assess the indirect regional environmental impacts of economic

energy storage operation.

The allocation of energy storage systems (ESSs) in distribution systems for voltage support under high penetration solar PV is investigated. A genetic algorithm based bi-level optimization method is developed that reduces the voltage fluctuations caused by PV penetration through deploying ESS among permitted nodes of a distribution system while accounting for their capital, land-of-use, and installation costs using a qualitative cost model.

A convex optimization based charge/discharge scheduling algorithm for distributed ESSs co-located with solar PV systems is developed. The daily charge/discharge schedules reduce (1) peak net demand (that is, load minus PV generation) of the customer, (2) power fluctuations in the customer net demand profile, and (3) the reliance of the customer on the grid by way of promoting self-consumption of local solar PV generation. Moreover, a novel idea of a "supply charge" tariff that incentivizes ESS customers to store excess solar PV generation that may otherwise result in reverse power flow in the distribution grid is investigated. Introduction of a supply charge successfully reduces the maximum solar PV power supply to the grid and does not financially impact ESS owners.

Finally, the economic and emissions effects of residential ESS operation for cost minimization in each of the eight regional electric reliability entities of the contiguous U.S. is investigated. It is observed that the overall economic performance and environmental impact of ESS varies considerably from region to region and is driven most by regional emissions and utility tariff structure. Results indicate that policy makers seeking emission reductions should carefully consider the interaction between emissions and rate structure in future orders for net metering and residential rate reform.

Introduction

The objectives of this dissertation are to investigate how energy storage technologies should be allocated and operated to mitigate the impacts of variable solar PV resources in distribution systems while providing economic incentives for storage owners, and to assess the regional environmental impacts of economic energy storage operation. Chapter 1 describes a bi-level optimization method that reduces the voltage fluctuations caused by PV penetration through deploying BESS among permitted nodes of a distribution system while accounting for their capital, land-of-use and installation costs using a qualitative cost model. The optimization method is based on a genetic algorithm (GA) that uses a linear programming (LP) routine that minimizes the daily coincident peak demand. Chapter 2 develops a convex optimization (CO)-based charge/discharge scheduling algorithm for distributed ESSs co-located with solar PV systems. The CO-based scheduling algorithm minimizes the monthly electricity expenses of a customer who owns an ESS and incorporates both a time-of-use volumetric tariff and a demand charge tariff. This chapter also presents the novel idea of a "supply charge" tariff that incentivizes ESS customers to store excess solar PV generation that may otherwise result in reverse power flow in the distribution grid. The economic and emissions effects of residential energy storage operation for cost minimization service in each of the eight regional electric reliability entities of the contiguous U.S. is investigated in Chapter 3. The CO-based scheduling algorithm from Chapter 2 is used here to determine the optimal economic behavior of consumers. Concluding remarks are made in Chapter 4.

The text and data in Chapter 1, in full, is a reprint of the material as it appears in "Siting and sizing of distributed energy storage to mitigate voltage impact by solar PV in distribution systems", Babacan, Oytun; Torre, William, Kleissl, Jan, *Solar Energy*, 146 (2017), 199-208. The dissertation author is the primary investigator and author of this article.

The text and data in Chapter 2, in full, is submitted for publication of the material with the title "Distributed energy storage system scheduling considering tariff structure, energy arbitrage and solar PV penetration". Babacan, Oytun; Ratnam, Elizabeth L.; Disfani, Vahid R.; Kleissl, Jan. The dissertation author is the primary investigator and author of this article.

Chapter 3, in part, is currently being prepared for submission for publication of material. Babacan, Oytun; Hanna, Ryan; Abdulla, Ahmed; Kleissl, Jan; Victor, David. The dissertation author is the primary investigator and author of this article.

Chapter 1

Heuristic Optimization to Optimize Energy Storage Sizing and Siting on Distribution Feeders

1.1 Introduction

Grid-connected solar photovoltaic (PV) is among the fastest growing renewable power generation technologies. Estimated global capacity additions for solar PV exceeded 40 GW_{dc} in 2014 of which 6.2 GW_{dc} PV installations happened in the United States. Approximately 20% of U.S. installations were residential PV (REN21, 2015; GTM Research and SEIA, 2015).

In the face of widespread distributed solar PV adoption, existing distribution systems are often not ready for such transformation. Distribution systems are traditionally structured and operated assuming power flowing from the distribution substation towards commercial and residential customers. As penetration levels of PV increase power flow direction can reverse, potentially causing power quality, protection, and reliability issues due to local and intermittent electricity generation during daytime.

Commonly observed impacts with grid-connected solar PV include over-voltage issues at the network connection points, voltage fluctuations due to intermittent local power injections, and reversed power flow from load points. Baran et al. (2012) provides

a comprehensive reference on operation and protection issues on distribution systems under high PV penetration.

In most distribution systems, on-load tap-changing transformers (LTC) at the substation are used to control the network voltage magnitude within permitted limits. Traditionally, the DSO sets the tap setting of the distribution transformer sufficiently high to ensure voltage at a feeder's end is within limits (Carvalho et al., 2008). However, high PV output usually coincides with low residential load demand—typically during the middle of the day. This coincidence can cause voltage excursions at the end of the feeder exceeding acceptable limits. Therefore, as PV penetration in a distribution network increases, one single tap setting or even one single voltage regulator is unlikely to maintain acceptable voltage quality at the end of a feeder. In addition, passing clouds can cause PV generation to drop significantly and hence voltages to drop as well since PV output is no longer increasing the voltage level. This intermittent nature of PV generation can cause fluctuating voltages.

In addition, LTCs have a delay. They depend on mechanical devices that switch between taps to change the effective transformer turn ratio while maintaining a continuous current path—a sequential tap-change process that requires several seconds to move each tap. Therefore, these devices are not suitable for addressing fast-occurring voltage fluctuations (Baran and El-Markabi, 2007; Kabiri et al., 2014). Furthermore, voltage regulators on the distribution circuit usually depend on the local current measurements to estimate the voltage drop downstream on the feeder. When a significant part of the load on a feeder is supplied by local power generation, conventional voltage control cannot be executed effectively without additional measurements from the feeder (Baran and El-Markabi, 2007).

Addressing these technical issues usually requires costly distribution reinforcements. Nevertheless many technologies available today, such as smart inverters and

battery energy storage systems (BESS), are able to mitigate many of the adverse impacts of distributed solar PV penetration. Most methods to buffer PV impacts on distribution systems utilize real power and/or reactive power injections or absorptions (Alam et al., 2012).

This work addresses the "BESS allocation problem"—that is, the issue of locating, and sizing BESS—to reduce voltage fluctuations caused by distributed PV through real power injections and absorptions by BESS. Optimal allocation and operation of these systems is an important task in distribution system engineering since deployment of these systems is capital intensive. The solution space of BESS allocation in distribution systems is fairly large and discontinuous. This optimization problem is usually nonlinear, stochastic, highly constrained, multi-objective and multi-modal (Moradi and Abedini, 2012; Morvaj et al., 2016). Hence the optimization problem in hand is hard to solve. An exhaustive enumeration of all possible solutions is guaranteed to give an optimal solution, but the size of the problem makes this approach computationally prohibitive.

As an alternative to prohibitive exhaustive methods, heuristics are a class of search methods that consist of sets of rules for deciding how the search will be done in a search space to find the global optimal value. Population-based stochastic optimization techniques such as Genetic Algorithms (GA) are an accepted and widely used method in literature to model distributed generation (DG) and BESS allocation optimization (Celli et al., 2005; Borges and Falcão, 2006; Chen et al., 2011; Moradi and Abedini, 2012). Their ability to form a diverse solution set via an iterative solution process makes these techniques capable of coping with large and discontinuous search spaces. Therefore, in this work a GA-based bi-level optimization method for BESS adoption is formulated to minimize voltage fluctuations in a distribution network caused by intermittent solar PV systems. The goal of this work is to understand the benefit of BESS in distribution networks with high PV penetration. A particular interest is to understand how sizing and

siting influence the overall benefit of BESS.

There have been several attempts to investigate aspects of sizing and siting problems. Many of the works (Celli et al., 2009) primarily focus on direct economic gains such as minimizing the electrical network losses without considering ancillary BESS services and many others (Atwa and El-Saadany, 2010) often do not use a formulation that solves siting and sizing problem simultaneously. Moreover, studies utilizing stochastic methods (Moradi and Abedini, 2012; Chen et al., 2011) usually lack validation studies to showcase the performance of their algorithm in finding near-optimal ("good") solutions. This study contributes to the literature by providing a methodology and analyses to overcome these drawbacks by formulating an objective function that is based on the trade-off between costs associated with sizing and siting of BESS and grid health benefits gained through mitigation of voltage fluctuations. In addition, the work presented here includes a detailed validation study to showcase the algorithm's ability to reach global optimality.

1.2 Methodology

1.2.1 Problem formulation

The optimization goal in this study is to effectively site and size BESS for a distribution system to mitigate voltage fluctuations caused by distributed solar PV systems. The scenario can be summarized as following: In a given distribution system, customers are adopting solar PV systems, so planners need to decide where a BESS should be located (siting) and what capacity of a BESS would be needed at that location (sizing) to mitigate voltage excursions caused by the newly adopted solar PV systems. This scenario is referred to as the "allocation problem" throughout the paper. Without loss of generality, we assume the following conditions to set up the allocation problem:

- Solar PV is allocated randomly within the distribution system. Its power rating is sized to the peak demand of the customer at the installation point. Existing systems are kept fixed and new systems are randomly added to other locations to accommodate higher PV scenarios.
- The Global Horizontal Irradiance (GHI) profile of each PV system follows a single global GHI curve (spatial uniformity in solar resource).
- The load profile of each customer follows a global demand curve. (spatial uniformity in demand)
- The reference distribution system is assumed to have no BESS.
- BESS installations are restricted to primary lines in the distribution network.
- A *perfect* daily forecast for solar and load profiles is input into the optimization (i.e., perfect information). No forecast errors are taken into consideration in order to decouple the performance of the allocation algorithm from the performance of the BESS dispatch routine, which, in turn, is sensitive to forecast errors (Hanna et al., 2014).
- Each BESS starts the day with 20% state of charge (their reserve energy) and returns to that reserve energy at the end of the day. This ensures that no energy-shift occurs between days, possibly creating a benefit bias in multi-day simulation results compared to single-day simulation results.
- The dispatch signal for energy charge/discharge is optimized for system-level peak demand reduction, i.e. it is identical for all BESS.
- Existing voltage regulators and capacitors operate with respect to their usual operation parameters.

These assumptions change the final siting and sizing decisions, but do not affect the working principles of the algorithm.

1.2.2 Objective function

The optimization is formulated with two decision variables: BESS capacity and network installation node. The term "BESS configuration" herein refers to a set of BESS fleet configurations determined by these two decision variables. The single objective optimization is then expressed as:

$$\max \quad \lambda_{\text{cost}} \cdot \bar{V}_{\text{dev-reduction}}\,, \tag{1.1}$$

where

$$\lambda_{\text{cost}} = f(n_s, k_s)\,,$$
$$\bar{V}_{\text{dev-reduction}} = f(n_s, k_s)\,,$$

and such that n_s is a set of nodes l_i in a distribution system with m number of BESS, i.e. $n_s = \{l_1, \ldots, l_m\}, \forall l_i \in \mathbb{N}_{>0}$, k_s is the set of the energy and power ratings k_i of each respective BESS[1], i.e. $k_s = \{k_1, \ldots, k_m\}, \forall k_i \in \mathbb{R}_{>0}$, and both sets belong to the set C that contains all possible combinations of set of values, i.e. $\{n_s, k_s\} \in C(N_{all}, K_{all})$. $\bar{V}_{\text{dev-reduction}}$ quantifies the reduction in total voltage fluctuation achieved through adoption of the BESS fleet configuration. λ_{cost} is a multiplier that penalizes the objective function for large aggregate system capacity and large total number of systems in the BESS fleet configuration. In the following section these two objective terms are further detailed.

[1] For the remainder of this work energy and power ratings of each BESS will be considered equal and the energy rating will be referred as *BESS capacity* in kWh.

Calculating voltage fluctuations at local PV generation nodes

Voltage fluctuations are caused by local variations in power supply and/or demand. A literature review reveals a wide variety of metrics to calculate voltage fluctuations. To the knowledge of the authors, there is no consensus for quantifying voltage fluctuation impacts of DG (or BESS) in distribution networks. Several attempts to formulate voltage quality indices and metrics can be found in Chiradeja and Ramakumar (2004); Moradi et al. (2015); Moradi and Abedini (2012); Nick et al. (2014). These formulations include either computing the difference between fixed reference voltage or computing a voltage index by dividing voltage at each bus with and without distributed generators. Our formulation, which is partially inspired from such literature, focuses on voltage impacts from PV generation at each PV interconnection point and is presented here.

The voltage fluctuation caused by solar PV is measured at each distribution system node n against a reference voltage $V^{\text{ref}} = 1\text{pu}$ that is independent of time step i or node n —i.e. the reference voltage is permanent and uniform. The voltage fluctuation is computed at all nodes based on this per unit voltage difference:

$$\begin{aligned} \Delta V_{n,i}^{\text{pv}} &= |V_{n,i}^{\text{pv}} - V^{\text{ref}}| \quad , \\ \Delta V_{n,i}^{\text{pv+es}} &= |V_{n,i}^{\text{pv+es}} - V^{\text{ref}}| \, . \end{aligned} \tag{1.2}$$

At each time step i, the voltage fluctuation at each node n in the *pv* case is ranked based on magnitude—from highest to lowest per unit voltage difference: $|\Delta V_{n,i}^{\text{pv}}|_{\text{ranked}}$. The top of this ranked node set for the *pv* case is designated as "critical nodes". That sorted order is then applied to the *pv+es* case to obtain the voltage variation at the same nodes: $|\Delta V_{n,i}^{\text{pv+es}}|_{\text{ranked}}$. The number of critical nodes ζ is selected to be equal to the total number of installed PV systems in the network.

The objective function considers only these critical nodes so that the voltage

fluctuation metric is not averaged out by less-effected nodes (typically located far from PV systems) and BESS siting is more strongly coupled to the largest points of fluctuation. Voltage fluctuation rankings are re-evaluated at each time step. Thus, the critical node designation changes as different nodes of the distribution system are getting impacted differently during the day. In this way, the objective function aims to diminish the extreme fluctuations among all of the nodes during the course of the day.

The effect of the BESS fleet is calculated by taking the ratio of root mean square differences from V_{ref} for the *pv* and *pv+es* cases. The resulting ratio is subtracted from unity so as to produce positive values in the case when BESS improves the voltage profile —i.e. when its operation reduces the voltage fluctuations. The summation of this value over the scheduling horizon of 1 day gives the total improvement (positive value) or adverse impact (negative value) of the BESS fleet:

$$\bar{V}_{\text{dev,reduction}} = \sum_{i=1}^{T} \left(\frac{V_{\text{dev},i}^{\text{pv}}}{V_{\text{dev},i}^{\text{pv+es}}} - 1 \right), \tag{1.3}$$

where $V_{\text{dev},i}^{\text{pv}} = \sqrt{\frac{1}{\zeta-1} \sum_{n=1}^{\zeta} (V_{n,i}^{*\text{pv}} - V^{\text{ref}})^2}$, $V_{\text{dev},i}^{\text{pv+es}} = \sqrt{\frac{1}{\zeta-1} \sum_{n=1}^{\zeta} (V_{n,i}^{*\text{pv+es}} - V^{\text{ref}})^2}$ at each time step i, $V_{n,i}^{*\text{pv}}$ and $V_{n,i}^{*\text{pv+es}}$ are the ranked node sets for *pv* and *pv+es* cases at each time step i and ζ is the number of critical nodes.

The implementation of Eq. (1.3) is illustrated in Fig. 1.1. In the *pv* case solar PV systems generate power according to the solar power profile shown and inject real power locally. The *pv+es* case is then calculated according to the given BESS charge and discharge signal. Finally, the resulting V_{dev} values of each case are used to compute $\bar{V}_{\text{dev,reduction}}$ given in Eq. (1.3).

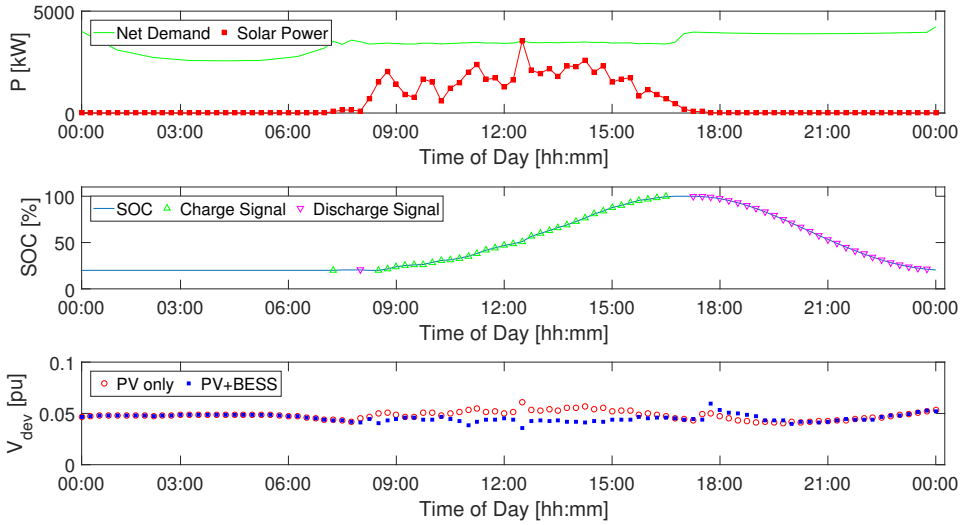

Figure 1.1. Overview of a typical daily simulation. The simulation shown has 50% PV penetration on a partly cloudy day (February 16th, 2014) (top) Aggregate net demand (Load minus PV minus BESS) and solar power generation. (middle) Cumulative BESS state of charge and charging and discharging signals. (bottom) Voltage fluctuation of *pv* only and *pv+es* cases calculated with respect to 1pu.

Assessing the economic performance of the fleet

A qualitative BESS cost model enters the objective function as a multiplier, λ_{cost}, that penalizes larger BESS capacity and more BESS sites. λ_{cost} represents capital costs qualitatively but could be also reconfigured into a monetized cost model that reflects specific market characteristics. Since dispersed large BESS fleets better mitigate the local voltage fluctuations than centralized small BESS fleets, λ_{cost} introduces a trade-off between the benefit of voltage fluctuation support and the cost of introducing more and/or larger BESS into the circuit.

The cost model is expressed as:

$$\lambda_{\text{cost}}(n_s,k_s) = \left(\frac{p_0}{l_{k_s}}\right)^{c_1} - c_1 \cdot p_1(l_{k_s} - p_0) - c_2 \cdot (l_{n_s} - 1)\,, \tag{1.4}$$

where p_0 is the smallest permissible BESS capacity, p_1 is a constant scaling and also unit conversion parameter between kWh to MWh, c_1 is the sizing cost parameter, c_2 is the siting cost parameter, l_{k_s} is the total installed BESS capacity in kWh and l_{n_s} is the number of BESS installed. The behavior of λ_{cost} is illustrated in Fig. 1.2.

The reference point of the cost model case $\lambda_{\text{cost}}(1, p_0) = 1$ is a single BESS installed with the smallest permissible capacity. In relative to this reference point, the cost model then penalizes the objective function with increasing BESS capacity and increasing number of BESS installations.

The first two terms in Eq. (1.4) penalizes the objective function for larger aggregate BESS capacity. As l_{k_s} increases, λ_{cost} decreases, reflecting the increasing capital cost of installing larger BESS. The first term (black dashed line in Fig. 1.2) represents an increasing scale of operation in capacity where marginal capital cost is decreasing when larger BESS is purchased, i.e. *decreasing marginal cost of adding*. As l_{k_s} gets very large, the per unit cost of additional units becomes constant due to a minimum expenditure required independent of the quantity purchased, i.e. *constant marginal cost of adding*.. This behavior is captured by the second term (cyan dashed line in Fig. 1.2)

The last term in Eq. (1.4) penalizes the objective function for having more BESS installations in the circuit. Unlike the first and second terms explained above, the siting penalization is linear assuming land-of-use costs do not increase as some of available sites are getting occupied and installation costs are constant per each additional BESS site. The effect of the siting cost parameter is seen in Fig. 1.2 as blue lines extending linearly below the purple line.

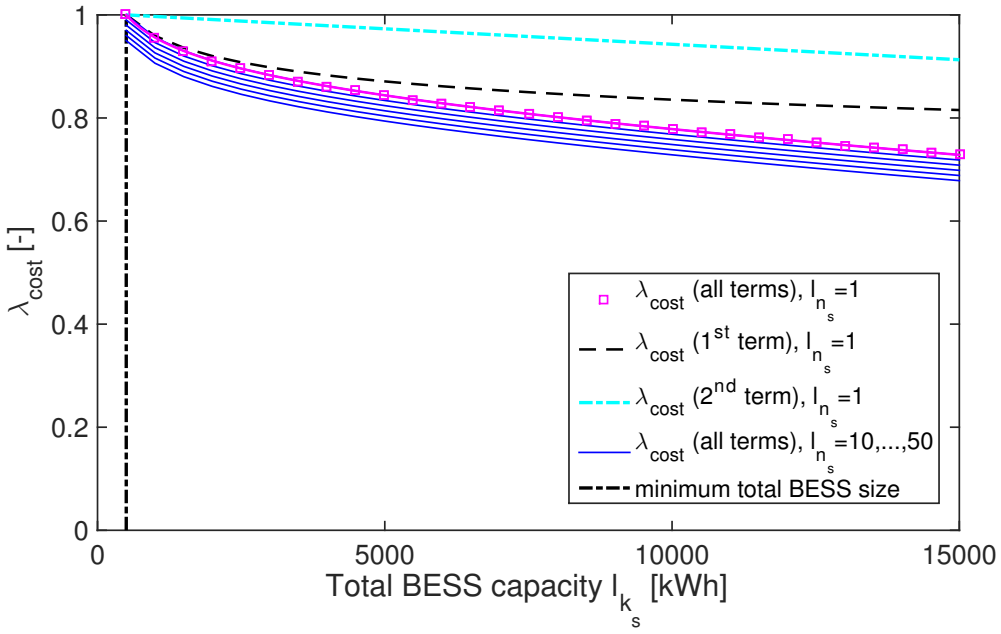

Figure 1.2. Cost penalty multiplier λ_{cost} illustrated with the following parameters: $p_0 = 500$ kWh, $p_1 = 10^{-4}, c_1 = 0.060, c_2 = 0.001$. The larger λ_{cost} the lower the cost. Cumulative BESS capacity is varied between 0 MWh and 15 MWh, which is the typical range for the IEEE8500 case study simulations. The purple line shows the centralized case with a single BESS location resulting in the lowest cost possible for each BESS capacity and neighboring parallel blue lines show increased penalty as the number of BESS installations are increased from 10 to 50 by 10 increments. The black and cyan lines depict the 1st and 2nd term of Eq. (1.4), respectively.

Constraints

There are two sets of constraints used in this study— one for main level optimization and the other for the secondary level optimization. Main level constraints are defined as: (1) set of nodes in distribution system where it is permissible to install a BESS and (2) the smallest permissible BESS capacity per node, i.e. the resolution of BESS capacity. The secondary level constraints consist of the BESS constraints; i.e. capacity, initial state of charge, state of charge limits, maximum discharge rate and minimum charge rate.

1.3 Implementation of the allocation problem

1.3.1 Overview of the implementation

The allocation problem is structured as a bi-level optimization (Figure 1.3). The overview of the model is given in Fig. 1.3. The main level conducts the siting and sizing optimization of the BESS fleet, while the secondary level conducts the operational optimization of each BESS. A GA is formulated to cope with the combinatorial complexity of the allocation problem.

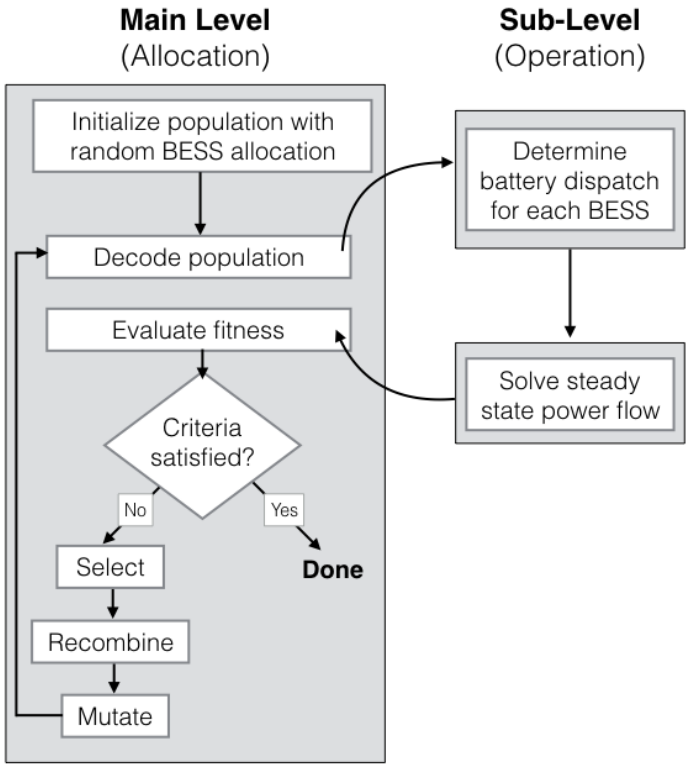

Figure 1.3. Bi-level optimization method overview. The main level algorithm optimizes the allocation of the BESS fleet. At the step where the current population is decoded, each solution set is sent to the sub-level optimization where BESS dispatch curves are determined for each BESS available. The power flow analysis is then conducted using these BESS dispatch curves and the power flow metrics are passed back to the main level optimizer to evaluate the fitness value of each solution. The main level algorithm is executed in loops until a termination condition is reached.

In the secondary level the operating schedule of each BESS is determined by a linear programming (LP) routine that minimizes the daily non-coincident peak demand (Hanna et al., 2014). Example dispatch signal for a given demand and solar power profile is illustrated in Fig. 1.1. Power flow simulations are conducted using OpenDSS (Electric Power Research Institute, 2008), an open source electric power distribution system simulator.

1.3.2 Formulation of the Linear Program

The LP routine used in the bi-level optimization method receives solar power and load forecasts as its inputs and sets a load demand target. The primary goal of the LP is the daily minimization of peak non-coincident demand.

The load demand target is to minimize demand using solar PV and BESS adjusted throughout the day in response to forecast error. In this study, solar PV power and load data are provided to the LP routine as perfect forecasts, and consequently BESS dispatch is not affected by forecast error. The mathematical formulation of the LP is as originally presented in Hanna et al. (2014).

1.3.3 Formulation of the Genetic Algorithm

GA is a stochastic and iterative global search method. GAs are well-suited to solving discontinuous functions, and hence the allocation problem in this work. In the following sections the details of the GA formulation developed in this work will be given along with several fundamental GA terminology in order to help readers with limited familiarity with GA.

The GA routine starts with an initial collection of potential solutions $P_0 = \{x_1^0, \ldots, x_n^0\}$, i.e. an *initial population*. This initial population will produce new collections, *generations*, throughout the optimization procedure with some transition rule

τ in an iterative manner: $P_0 \xrightarrow{\tau} P_1 \xrightarrow{\tau} P_2 \xrightarrow{\tau} \ldots$. The resulting generations will be represented as $P_t = \{x_1^t, \ldots, x_n^t\}$ where t is the iteration step. Each solution x_i^t is evaluated with respect to the objective function of the problem. This value, called the *fitness value*, is a measure of fitness for each solution. Then, a new collection of solutions, a new *generation*, is formed by selecting the fitter solutions, i.e. fitter *individuals*, by means of genetic operators –*selection*, *recombination* and *mutation*– until the algorithm converges to a final solution. The combination of these genetic operations is considered as the transition rule τ. Since genetic operators are in general nondeterministic, simulations with identical initial conditions may not result in the same outcome. The GA iterates until a preset termination condition is reached. The GA formulated in this study consists of recipes for a classical genetic algorithm. The complete set of recipes are as follows: method of representation, method of selection, method of recombination, method of mutation, method of termination. The following section explains each of these in turn. The notation used in this section is drawn primarily from Back (1996); Vose (1999); Rothlauf (2006).

Method of Representation

GA works in a *genotypic domain* to which potential solutions are uniquely mapped using an *encoding alphabet*. This encoding alphabet is binary in this study. All genetic operations are done in this genotypic domain. The solutions are then decoded into the *phenotypic domain* to obtain their fitness values. In our study, the phenotype - genotype mapping transforms BESS energy and power ratings into binary strings. All binary strings are then aggregated into a single binary string while preserving the network node location information appropriately.

Mathematically, each integer value of BESS capacity $x_p \in \{1, 2, \ldots, BESS_{rating,max}\}$ is represented by a binary string x_g of length $l = log_2(BESS_{rating,max})$. The genotype -

phenotype mapping J_g is then defined as

$$x_p = J_g(x_g) = \sum_{i=0}^{l-1} 2^i x_{g,i}, \tag{1.5}$$

where $x_{g,i}$ denotes the ith bit x_g.

The binary representation of integer values limits the GA search to discrete grid points in the continuous solution space. In our allocation problem, the integer representation implies that BESS ratings are discretized in 1 kWh/1 kW increments, which is a sufficiently high resolution for the nature of the problem.

Method of Selection

GA formulations utilize either a proportional or a ranking selection scheme. Proportional selection scheme mechanisms fail in presence of negative fitness values and thus require an additional scaling operation before selection. However, this scaling technique might in return manipulate the selection probabilities of individuals (Vose, 1999). Since the objective function proposed in this study can compute negative fitness values, a ranking selection scheme is chosen over proportional.

Tournament selection is utilized as it has been proven to work well (Srinivas and Deb, 1994; Horn et al., 1994). In tournament selection, a tournament between u randomly chosen different individuals is held and the fittest individual is chosen with a probability p_s. After v tournaments of size u, the mating pool is formed. Here, a tournament selection with replacement is being used, i.e. all individuals in the population are considered for every tournament regardless of the fact that they might have been chosen before. After v tournaments the mating pool is filled with n individuals. The selection in this study is stochastic, i.e. p_s is not equal to 1 and individuals with smaller fitness values can be still chosen over the others. This ensures that the population is diverse over many generations and avoids premature convergence to a local solution.

Method of Recombination

One of the main principles of GA is explained by the Schema Theorem. In simple terms, the short useful information segments, so called *building blocks*, of earlier solutions might lead to longer information segments of high fitness values in later iterations (Mitchell, 1998). This idea can be easily extended to the allocation problem. Certain nodes in distribution systems (short useful segments in genotypic representation, i.e. bit strings) are favorable for BESS over other nodes. The solutions with these nodes are likely to have a higher fitness value than solutions that lack these nodes. By passing these favorable nodes to new candidate solutions, an overall good solution is expected to emerge in later generations.

The recombination ensures this crucial exchange of building blocks between different individuals. In this study, among two randomly selected solution sets x_{p1} and x_{p2}, the uniform crossover operator chooses whether the selected solution sets should exchange information with a probability p_c. An exchange swaps the bit i between both individuals until each bit i is processed:

$$\begin{aligned} x_{p1} &= (x'_{g,1},\ldots,x'_{g,i},\ldots,x'_{g,l}), \\ x_{p2} &= (x''_{g,1},\ldots,x''_{g,i},\ldots,x''_{g,l}), \end{aligned} \tag{1.6}$$

and

$$\begin{aligned} x_{c1,i} &= \begin{cases} x'_{g2,i}, & \text{if } \chi_i > p_c \\ x''_{g1,i}, & \text{if } \chi_i \leq p_c \end{cases}, \\ x_{c2,i} &= \begin{cases} x'_{g1,i}, & \text{if } \chi_i > p_c \\ x''_{g2,i}, & \text{if } \chi_i \leq p_c \end{cases}, \end{aligned} \tag{1.7}$$

where $\forall i \in \{1,\ldots,l\}$ and $\chi_i \in [0,1]$ denotes a uniform random variable generated for each bit. The result of the recombination is two new child individuals, x_{c1} and x_{c2}, created by crossing over two parent individuals, x_{p1} and x_{p2}, selected at random from the population.

Method of Mutation

The mutation operator occasionally disturbs the bit structure of randomly selected individuals. This random process introduces significant changes in a few individuals in hopes of exploring other yet unknown parts of the search space. If the change improves the fitness value of the individuals they are likely to be passed to emerging generations. This operator helps the GA routine to avoid getting stuck at only locally optimal regions of the solution space.

In this study, the mutation operator goes over each bit of an individual and applies a bit inversion with a probability p_m. Each bit string x'_g of the new individual is:

$$x'_{g,i} = \begin{cases} x_{g,i}, & \text{if } \chi_i > p_m \\ 1 - x_{g,i}, & \text{if } \chi_i \leq p_m \end{cases}, \tag{1.8}$$

where $\forall i \in \{1,\ldots,l\}$ and $\chi_i \in [0,1]$ denotes a uniform random variable generated for each bit.

Method of Termination

The following termination or convergence criteria are used for the simulations:

- The total number of new populations reaches a preset limit.
- The fitness remains the same for a preset number of generations.

- The siting decision remains unchanged for the fittest individual for a preset number of generations.

1.3.4 Parameterization of the GA

GA parameters are determined following common practice in the literature and later calibrated by numerous tuning simulations tailored for our algorithm. The tuning simulations are conducted by running simulations with all possible parameter combinations within permissible ranges while observing which combination of parameters results in the best performance. This section lists all parameters required to reproduce the GA routine.

The GA routine initializes 120 solution sets, or *individuals*, by uniformly distributing the number of BESS (a maximum of 7) and the cumulative BESS capacity (the initial maximum capacity equals to the total PV system capacity in kVA) in the fleet. These systems are then sited randomly among permissible nodes. The optimization routine does not restrict the rating of BESS that might be installed in the circuit. If favorable, the solution space may expand into larger BESS capacities compared to the initialization.

At each iteration, or *generation*, simulations for each individual are done using the solar irradiance time-series based on the weather condition of the simulation day. After computing the fitness value of each individual, the whole generation undergoes the GA operators: selection, crossover and mutation.

This study uses 2% elitism, i.e. in each generation, the fittest 2% of the individuals are guaranteed to pass to the next generation without being exposed to any of the genetic operators including mutation. The parameters in the tournament selection are set as the selection probability $p_s = 0.80$ and the tournament size $u = 2$.

Parameterized uniform crossover with a swapping probability p_c of 0.50 is ap-

Table 1.1. The results of the sensitivity simulations for varying PV penetration levels and the sizing and siting cost penalty parameters. The scenario column indicates the type of sensitivity study and the diamond symbols (♢) indicate the reference simulation with the default parameters that are kept the same across the 3 scenarios. L_{ALL} lists the aggregated BESS fleet capacity. # indicates the number of BESS installed. For each simulation type, the mean and standard deviation of BESS capacity in MWh are shown for each permissible distribution system node L_i among 5 representative final result, i.e. the best solution of 5 representative simulation. L_1, L_2, L_4 and L_5 are not shown here as they were not chosen for BESS procurement during these simulations.

Scenario	Variable	L_{ALL}	*BESS#*	L_3	L_6	L_7
PV penetration	PVP					
Low	10%	5.8 ± 0.0	1	-	5.8 ± 0.0	-
Moderate	25%	10.3 ± 0.1	2	-	5.2 ± 0.3	5.1 ± 0.3
High ♢	50%	15.0 ± 0.2	2	-	2.5 ± 0.5	12.5 ± 0.7
Cost of Sizing	c_1					
Low	0.040	17.3 ± 0.1	3	1.1 ± 0.1	1.5 ± 0.5	14.8 ± 0.8
Moderate ♢	0.060	15.0 ± 0.2	2	-	2.5 ± 0.5	12.5 ± 0.7
High	0.140	8.8 ± 0.1	1 or 2	-	1.4 ± 1.3	7.4 ± 1.4
Cost of Siting	c_2					
Low ♢	0.001	15.0 ± 0.2	2	-	2.5 ± 0.5	12.5 ± 0.7
Moderate	0.025	15.2 ± 0.4	1 or 2	-	1.6 ± 1.4	13.7 ± 1.7
High	0.050	15.4 ± 0.2	1	-	-	15.4 ± 0.2

plied for recombination. As first part of the mutation, 10 new randomly generated individuals are introduced in each generation. Random individuals are created, similar to the initialization, by uniformly distributing the number of BESS and the cumulative BESS capacity (maximum capacity equals total PV system capacity in kVA) in the fleet. After 10 generations, the mutation operation switches to an uniform bit string mutation with a probability p_m of 0.010.

1.3.5 Test circuit and data sources

The IEEE 8500-Node test feeder with balanced 120 V secondary loads on the service transformers is chosen as the benchmarking circuit. This circuit is a radial distribution feeder with multiple feeder regulators and capacitors (Arritt and Dugan,

2010) and is a suitable test feeder to assess the proposed algorithm as it is similar to a large feeder with many typical elements found in a residential distribution feeder.

The PV generation fleet is assumed to be composed of distributed rooftop systems located in direct proximity (i.e. secondary side of the service transformer) to respective load points. For each level of PV penetration, PV systems are sited randomly among the load points of the circuit until the desired penetration is reached. The initial PV system allocation is kept fixed for increased levels of PV penetration. Each system is specified to have a capacity equal to the peak demand of that bus.

Testing and demonstration of the algorithm is carried out using 15 minute resolution demand and solar generation data. Generic demand profiles for residential buildings in San Diego are imported from the dataset provided by Open Energy Information (Open Energy Information, 2014). PV power output data from 2014 are collected from a real PV systems located at the campus of University of California, San Diego campus. The PV system tilt angle and azimuth angles are 20° and 180° (due South), respectively.

1.4 Validation of the implementation

1.4.1 Validation approach

The goal of the validation is to understand the shape of the solution space and determine whether the GA routine can successfully identify the global peak region within this solution space. Exhaustive enumeration systematically computes the fitness values of all possible BESS fleet combinations among all permissible nodes but with a limited BESS capacity resolution at each permissible node. If this BESS capacity resolution was set to 1 kWh/1 kW increments at each permissible node, exhaustive enumeration would include all BESS fleet possibilities among which the GA routine is searching. However, this search space for exhaustive enumeration is computationally too costly.

Thus, a coarser BESS capacity resolution at each permissible node is determined so that it is computationally feasible to run enough exhaustive enumeration to explore the solution space at meaningful intervals. The resulting exhaustive enumeration approximates the real solution space with an acceptable degree of uncertainty.

In specific the capacity for each BESS is only allowed to change in large increments and siting is restricted to 7 nodes. The increments for each case are determined by dividing the total BESS capacity by the number of permissible nodes. Furthermore, the GA binary representation is also restricted to approximate similar incremental changes to that in the exhaustive enumeration. The details of this validation approach are given below.

The allocation problem in hand is analogous to the act of distributing a certain amount of balls into boxes. In this case, balls are BESS capacity that is to be allocated among certain network nodes, i.e. boxes. Then, the numerical burden of this problem equals to the total number of ways of distributing k balls into n boxes times the computation time per simulation. The following conditions are defined to complete the framework:

- Balls are indistinguishable from each other, i.e. they are identical. Similarly, BESS capacity is distributed among network nodes indiscriminately since BESS technology does not differ.
- Boxes are distinguishable from each other, i.e. the installation node of each BESS is important to distinguish in the allocation problem.
- Each box may contain more than a single ball, i.e. certain network nodes might have higher BESS capacity than the others.
- Some boxes may not receive a ball, i.e. certain network nodes might not be selected for any BESS installation during optimization.

Given the conditions above, the total number of permutations for allocation are

$$C(n,k) = \frac{(n+k-1)!}{(n-1)! \cdot k!}. \tag{1.9}$$

This relation reveals the numerical complexity of the exhaustive enumeration.

For the validation, the number of network nodes n can be chosen randomly as long as it is sufficiently numerous to avoid bias towards better performance. Example giving, limiting the number of available nodes to 2 or 3 locations would statistically increase the chances that the GA finds the optimal solution. On the other hand, increasing the number of nodes significantly increases the total required number of simulations. Considering this numerical trade-off, installations are limited to 7 network nodes in the benchmark network. The location of these nodes can be randomly picked as long as they are sufficiently distant from each other. The chosen node locations are shown in Fig. 1.4.

Validation simulations are conducted on the IEEE 8500-Node test feeder. For each BESS fleet capacity ranging from 5 MWh to 20 MWh the complete set of allocation possibilities is determined using the relation given in Eq. (1.9). The BESS capacity resolution is determined for each BESS fleet capacity by dividing the BESS fleet capacity by the number of permissible (7) nodes. Thus, the resolution for exhaustive simulations ranges from 714 kWh (in 5 MWh case) to 2857 kWh (in 20 MWh case). In contrast, the GA simulations have a constant finer BESS capacity resolution of 64 kWh.

1.4.2 Method validation results

The resulting maximum fitness value front of the solution space is shown in Fig. 1.5. The maximum fitness value front has a global maximum near 15.2 MWh with a fitness value of 4.40 and a local maximum near 17.5 MWh with a fitness value of 4.33. The best solutions determined by the 5 example GA simulations are shown

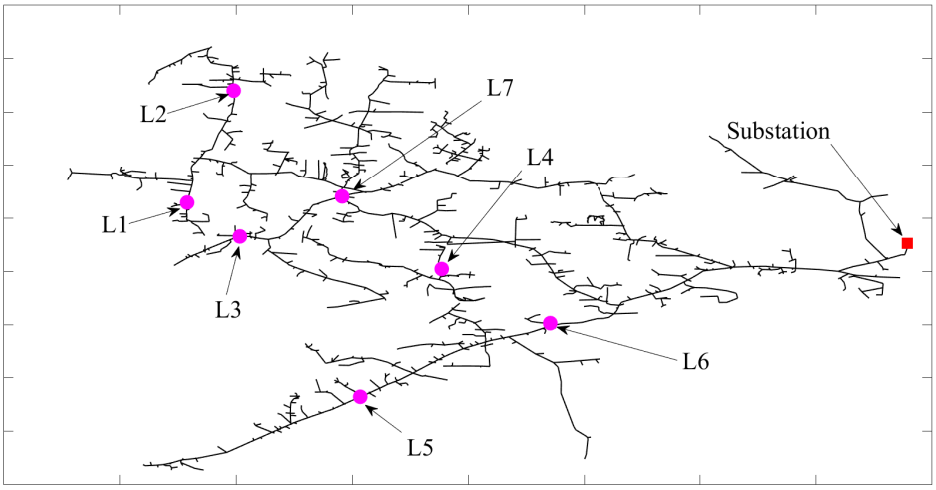

Figure 1.4. 7 distribution system nodes are chosen in the IEEE 8500-Node test feeder for validation studies. The node names are as follows; L1: M1009784; L2: M1027011; L3: M1026709; L4: M1047513; L5: M1069417; L6: E182748; L7: M1089145. The original IEEE 8500-Node test feeder used for the benchmarking studies for the allocation optimization method is described in Arritt and Dugan (2010).

in Fig. 1.5 as red crosses. The GA implementation is successful as each simulation identifies the region with the global maximum fitness (Fig. 1.5). The fitness values found in the GA simulations are larger than in the exhaustive simulation which is due to the finer BESS capacity resolution in the GA. The validation shows the success of the GA routine in arriving at the right sizing decision for the BESS fleet. A decisive conclusion on the validation also requires proof for consistent siting decisions among all of these simulation.

Figure 1.6 shows the location of each BESS installation decision made in the validation simulations. In all simulations the GA routine consistently converges to the same nodes, namely L_6 and L_7. The aggregate BESS capacity of each solution are consistent (see also Table 1) but individual decisions on different nodes differ indicating that similar cost-benefit relations can be achieved with slightly different combinations. The box plots of initial BESS capacities for each location demonstrate that results are insensitive to the initial conditions. For example, for node L_7 only two outliers out of a

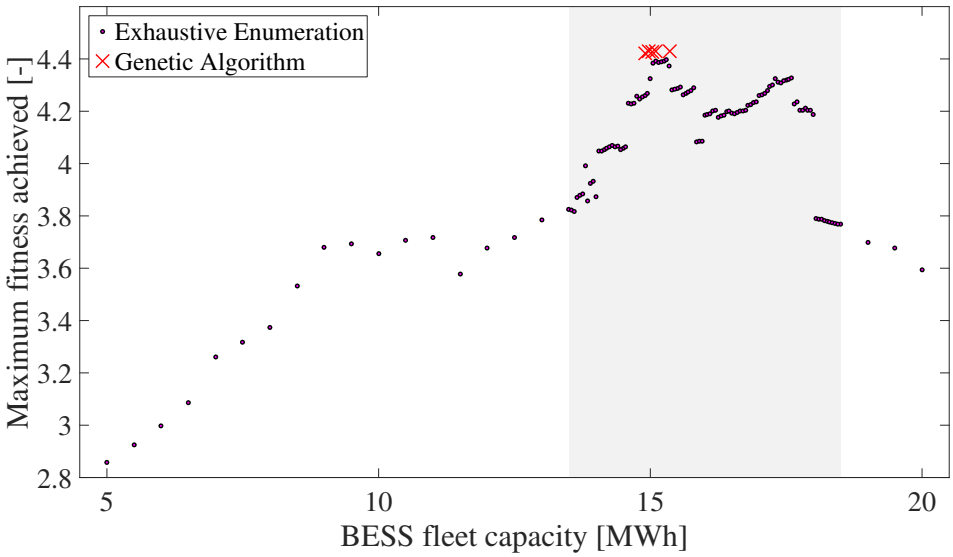

Figure 1.5. The maximum fitness values obtained for exhaustive enumeration. The resolution of the BESS fleet capacity within the gray box is 0.1 MWh, and 0.5 MWh elsewhere. The exhaustive enumeration peaks at 15.2 MWh with a fitness value of 4.40. The 5 example GA simulations shown here identified the best solution as 14.91 MWh with 4.42, 14.98 MWh with 4.43, 15.04 MWh with 4.43, 15.10 MWh with 4.43 and 15.36 MWh with 4.43. The respective siting decisions for these GA simulations are given in Fig. 1.6.

total of 600 initialized solutions have matching BESS capacities with the final decision. Moreover none of the initialized solutions have the exact combination of the final decision set, i.e. BESS installations only at L_6 and L_7. All of these arguments indicate that the proposed GA algorithm is able to make consistent siting decisions that also maximize the fitness value of the given objective function.

1.5 Sensitivity studies

Sensitivity studies are run for varying PV penetration levels as well as sizing and siting cost penalty parameters. The results of the sensitivity simulations are presented in Table 1.1. The simulations reached an optimal solution between 13 and 52 iterations. The mean of number of iterations until termination was 29.5 among all simulations. Figure 1.8 shows the mitigation of voltage fluctuations achieved in each scenario. The decrease

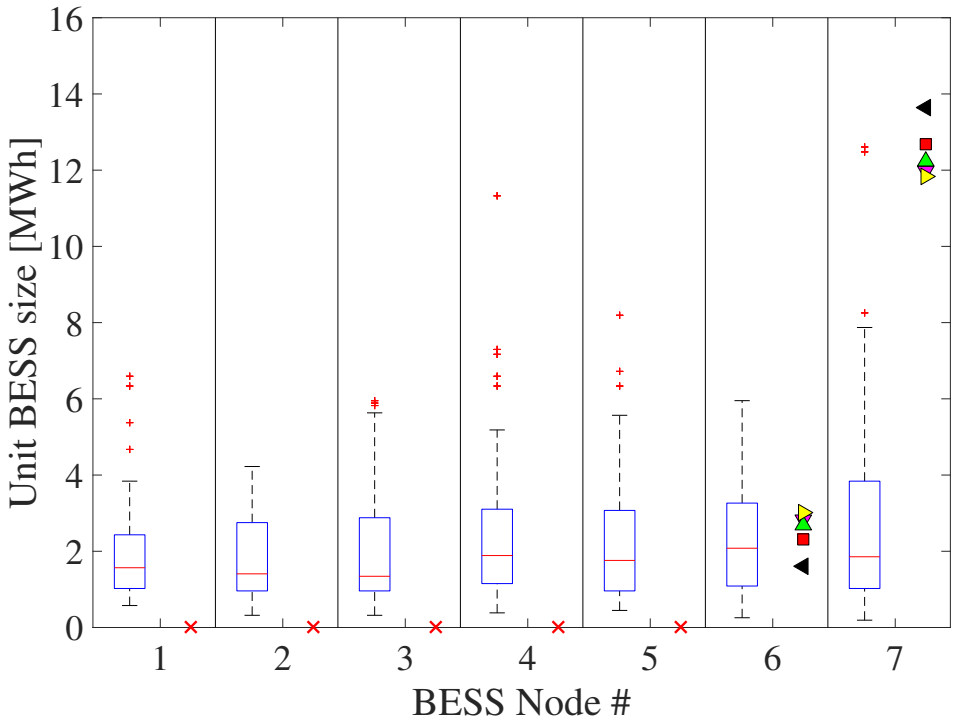

Figure 1.6. Comparison of method validation simulation initializations and results by BESS node. Box plots on the left side of each bracket show initialization for BESS capacities of 5 simulations. Red horizontal bars indicate the medians and red plus signs mark the outliers. On the right side of each bracket the final GA results are shown. There are no BESS installed at the nodes #1 through #5 (shown as red cross marks on the x-axis). Each individual GA simulation result for nodes #6 and #7 is shown with a different symbol and color.

in voltage fluctuations varies among scenarios considered. However, in all scenarios adopting BESS in the distribution system has a clear benefit in voltage mitigation.

The goal of these simulations is to understand whether the GA response to the changes in several key parameters is reasonable and to investigate the importance of these parameters for applications. Default parameters for the sensitivity study are given in Section 1.3.4. All simulations use these default parameters with the exception of the parameter under focus as indicated in the "Variable" column of Table 1.1. A representative sizing and siting result is shown in Fig. 1.7.

The top section of Table 1.1 shows that as PV penetration increases the aggregated

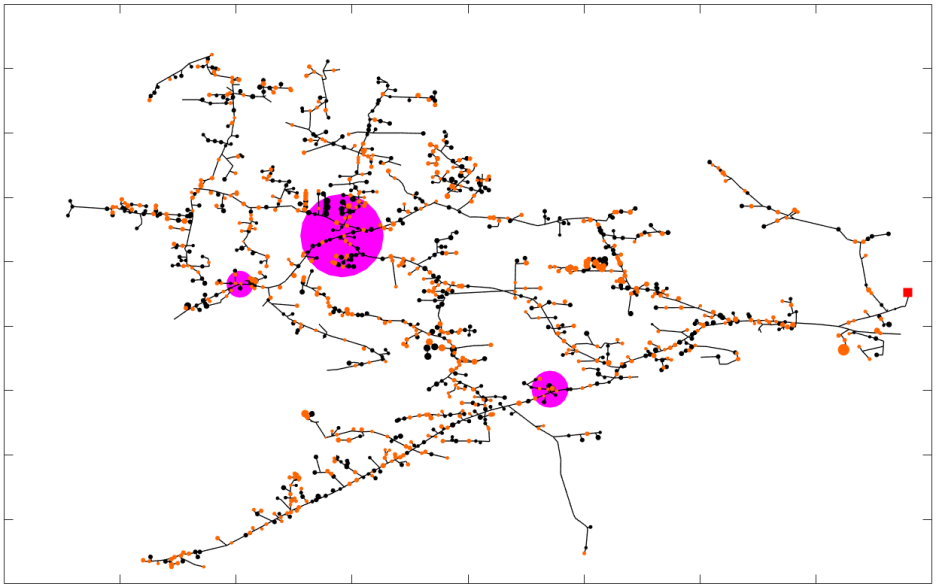

Figure 1.7. IEEE8500 test feeder one-line diagram and siting results of a representative simulation with 50% PV penetration for February 16th, 2014 (a partly cloudy day). The scenario is "Low cost of sizing" in Table 1.1 (First row of the middle section). Locations of proposed BESS units are marked with filled purple circles. Orange dots show loads with PV and black dots show load points without PV. Each dot is sized with respect to the capacity of the component.

BESS capacity, L_{ALL}, also increases. While the maximum number of nodes at which BESS can be installed is physically restricted by the permissible node set, the BESS capacity at each node is unlimited and a function of the cost-benefit relation. The observed BESS capacity increase is less than linear with increasing PV penetration.

Increasing the sizing cost penalty parameter results in a decrease in the aggregated BESS capacity, L_{ALL}, as expected. We also observe a decrease in the number of BESS installed in the distribution system. This change in decision is linked to the fact that even though there are many locations that could benefit from BESS, as the procurement of BESS becomes expensive, the less critically affected node L_3 is no longer supported. Instead, L_6 and L_7 are supported as much as possible with the available BESS in hand.

The bottom section of Table 1.1 investigates the effect of the siting cost parameter. Increasing the siting cost penalty parameter decreases the number of BESS installed

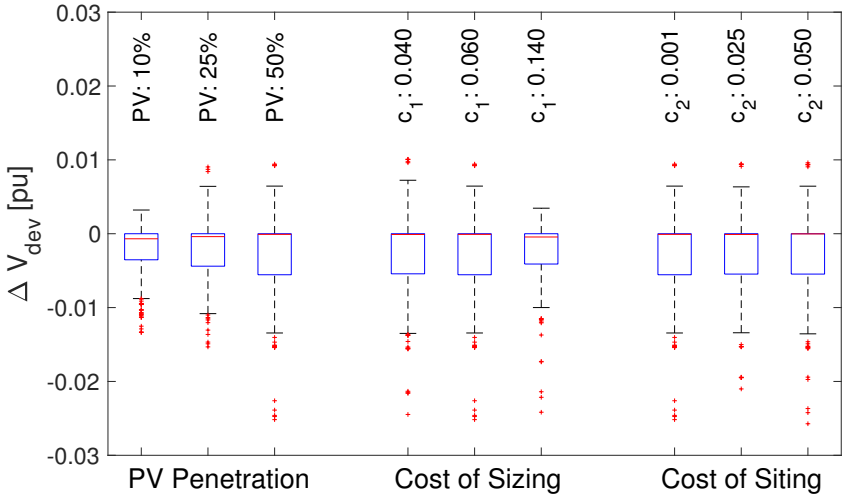

Figure 1.8. The mitigation of voltage fluctuations in the distribution system through BESS adoption under different case study scenarios. ΔV_{dev} is the difference of voltage fluctuations of *pv* only and *pv+es* cases as shown in Figure 1.1. $\Delta V_{dev} > 0$ indicates BESS operation increases the voltage fluctuation and $\Delta V_{dev} < 0$ indicates BESS operation mitigates the voltage fluctuations in comparison to *pv* only case. Each box plot is drawn for data sets covering all 5 final results presented for each case study scenarios in Table 1.1.

in the distribution system. This parameter does not have a significant impact on the aggregated capacity of the BESS fleet. As siting-related expenses become prohibitive, only the most affected node(s) receive a BESS. A small increase in the aggregated BESS capacity is observed as the fleet becomes centralized since the cost reduction obtained from centralization can be spent in increased BESS capacity.

These three sensitivity studies show that the optimization results qualitatively follow the design goals of the objective function given in Eq. (1.1).

1.6 Conclusions

This work described a methodology to optimally allocate utility-scale BESS to support high penetration solar photovoltaic integration in the distribution systems. The developed model consists of a genetic algorithm based bi-level optimization method that

dispatches each BESS for peak demand reduction. In practice technical, environmental or human factors greatly limited the eligible locations for utility-owned or operated BESS. The optimization algorithm can easily be modified to only accept a subset of the network for BESS siting and returns the feasible siting options and proper BESS sizing for the given permissible node set, demand and solar profiles, and the level of PV penetration in the circuit.

Benchmarking was carried out on the IEEE 8500-Node test feeder. The proposed method provides consistent solutions that appear to be optimal according to a validation against exhaustive enumeration of a simplified case. The simulations using a limited set of permissible system nodes successfully converge to consistent final solutions, both in sizing and siting.

The text and data in Chapter 1, in full, is a reprint of the material as it appears in "Siting and sizing of distributed energy storage to mitigate voltage impact by solar PV in distribution systems", Babacan, Oytun; Torre, William, Kleissl, Jan, *Solar Energy*, 146 (2017), 199-208. The dissertation author is the primary investigator and author of this article.

Chapter 2

Convex Optimization to Schedule Distributed Energy Storage For Cost Minimization and Ancillary Benefits

2.1 Introduction

Energy storage systems (ESS) are regarded as an enabling element of a future low-carbon electric grid as they allow higher amounts of renewable energy on the grid (DiOrio et al., 2015; de Sisternes et al., 2016). This stems, in part, from the operational flexibility ESS offer grid operators facilitating the integration of intermittent wind and solar power (Denholm et al., 2010). Increasing penetration of solar PV on the electric grid requires a new planning paradigm for capacity resources, which have traditionally been procured to meet system peak load and reserve requirements. Now, additional capacity is needed to provide flexible generation for integrating variable generation as well (Cutter et al., 2014). The proliferation of distributed ESS could provide this needed flexibility for a transforming grid.

With the rapid growth in grid-connected solar PV, electric utilities are facing stagnant electricity sales, particularly in the residential sector. This reduction in sales reduces the utility's ability to recover capital costs, which constitutes the majority of their expenses (McLaren et al., 2015). At the same time, the PV system owners still rely

on the grid for voltage and frequency control and for their night-time demand. They also need the grid to receive the economic benefit from exporting excess generation. However, as solar PV penetration in a distribution system increases, power flow direction can reverse, potentially causing power quality, protection, and reliability issues due to local and intermittent electricity generation during daytime (Baran et al., 2012).

Electric utilities might have difficulties addressing these problems without raising electricity rates. The ESS owners could be incentivized to support the electric grid through time-of-use tariffs and/or residential demand charges. Through demand charges the ESS owners have the opportunity to reduce their electricity bills by managing their demand and they also gain access to reduced electricity retail rates. In theory, demand charges improve load factor, reducing the need for new infrastructure investment, and result in an overall reduction in system costs. Residential demand charges are not a new concept but its application has been rare in residential tariffs so far. (Hledik, 2014).

There is an extensive literature on ESS charge/discharge scheduling for residential buildings that are coupled with a solar PV system. Several of these, e.g. (Moshövel et al., 2015; Luthander et al., 2016; Ren et al., 2016a), focus on increasing the consumption of solar PV generation locally and mitigating the peak power flows from and to the grid. However, they do not consider a demand charge tariff.

There are also a number of studies that consider a demand charge in their scheduling formulation. Geem and Yoon (2017) propose a population-based heuristic algorithm that reduces peak net demand of the customer and on-peak electricity purchases. Zheng et al. (2015) introduce a scheduling algorithm to reduce peak net demand and evaluates the economical feasibility of different energy storage technologies. Gitizadeh and Fakharzadegan (2014) formulate a Mixed Integer Linear Program (MILP) problem to optimize the capacity of ESS for peak net demand reduction and energy shifting. However, these studies fall short of demonstrating a robust stand-alone scheduling algorithm since

Zheng et al. (2015) and Gitizadeh and Fakharzadegan (2014) use a scheduling algorithm as a representative tool to investigate another research question, and Geem and Yoon (2017) do not present a comprehensive validation study of the algorithm.

In this work we present a convex optimization (CO)-based scheduling algorithm for distributed ESSs (Section 2.2) that incorporates both a time-of-use tariff and a demand charge tariff. The objective of the algorithm is to provide financial benefit to the ESS owner while inherently (1) reducing the peak net demand of the customer, (2) mitigating power fluctuations in the customer net demand profile, and (3) increasing local PV generation consumption for a co-located solar PV system. The ESS specifications, day-ahead load and solar forecast and the electric tariff are sufficient to deploy the algorithm on site. By means of a case study we benchmark the ability of the algorithm to minimize cost, reduce peak net demand, and mitigate net demand fluctuations, and compare it against two alternate methods proposed in the literature (Section 2.3 - 2.4).

In this work we also introduce a supply charge option in electricity rate offerings. A supply charge provides an incentive to customers to either self-consume PV generation, or to curtail their generation output when it exceeds their load requirements, thereby reducing the reverse power flow in the distribution grid. We discuss its impact on the grid, on the ESS cycling, and on the customer bill by comparing against a demand charge only case (Section 2.4). Section 5 concludes the paper.

2.2 Problem Formulation

2.2.1 Notation

Herein $\mathbb{R}^s$ denotes s-dimensional vectors of real numbers, where $\mathbb{R}^1 = \mathbb{R}$ and $\mathbb{1} \in \mathbb{R}^{s\geq 0}$ denotes the all-1 s column vector of length s. $s = 24\text{h}/\Delta t$ is the number of time steps in a day-long charging schedule, where Δt is the time-interval between consecutive

time-steps k in hours. $\mathbf{I}$ denotes the identity matrix of size s and $\mathbf{T} = [t_{ij}]$ denotes the s-by-s matrix satisfying $t_{ij} = 1$ for $i \geq j$ and $t_{ij} = 0$ elsewhere. We denote vectors in bold and represent matrices using uppercase bold characters.

2.2.2 Customer System Configurations

We model four system configurations shown in Figure 2.1 for customer-owned, grid-connected ESS, which might represent, for example, a residential household or a commercial business. Configurations a and b consist of an ESS and a customer load without PV. Configuration a prohibits the customer from selling electricity to the grid, whereas configuration b compensates the customer at the retail rate for delivering energy to the grid, thus allows energy arbitrage opportunities. Configurations c and d incorporate a customer-owned, grid-connected solar PV system into the configurations a and b, respectively. We assume customers with configuration c curtail solar PV generation when their energy storage is full and the solar PV system generation exceeds load, i.e. when net demand is negative.

For each system configuration, the power balance equation for the net demand $p(k)$ is given by

$$p(k) = l(k) - g(k) + c(k) - u(k) \tag{2.1}$$

for all time step indices $k \in \{1, ..., s\}$. All units are in kW. The average load of the system over a period Δt is $l(k)$, the average solar PV generation is $g(k)$, the average curtailed solar PV generation is $c(k)$, and the average ESS charge/discharge is $u(k)$, where $c(k)$ is zero for all time steps $k \in \{1, ..., s\}$ in configurations a, b and d, and $p(k)$ is nonnegative for all time steps $k \in \{1, ..., s\}$ in configurations a and c.

The constraint $p(k) \geq 0$ depicts the scenario where there is no financial incentive for energy to be sold to the grid. That is, in such cases curtailed solar generation $c(k)$ is equivalent to the excess PV generation that would have ordinarily been injected into the

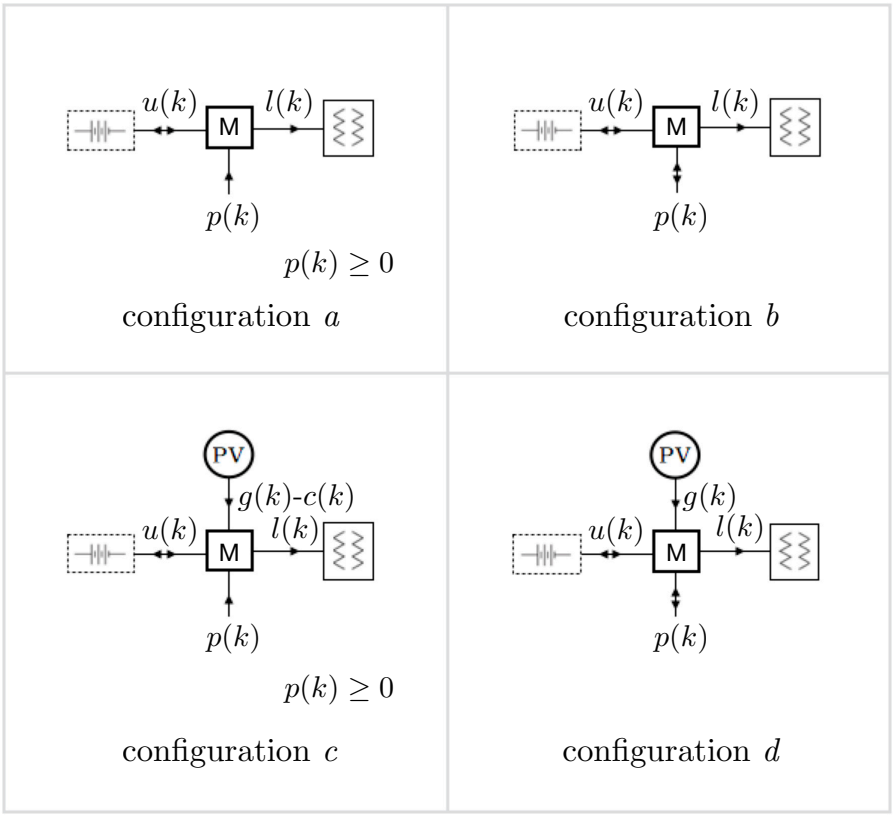

Figure 2.1. Configurations of the customer system under consideration. The average net demand over a period Δt is denoted $p(k)$ with k being the time step index, and is positive when flowing from the grid to the customer. The average ESS charge/discharge over Δt is denoted $u(k)$, and is positive when discharging. The average load of the system over Δt is $l(k)$. The average generated and curtailed power from the solar PV system over Δt is $g(k)$ and $c(k)$, respectively.

grid but this supply would not result in financial compensation to the customer.

2.2.3 Regulation and Accounting

A customer is billed monthly based on kWh electricity consumption via a *time-of-use* (TOU) tariff denoted by the length-s vector $\mathbf{\Lambda}_{\mathrm{e}} \in \mathbb{R}^s$. In addition, a net-metering program is considered in configurations b and d, in which a customer receives compensation for exported electricity at a rate equivalent to the TOU tariff.

We use two additional tariff mechanisms: A *demand charge* denoted by the scalar

Λ_d, and a *supply charge* denoted by the scalar Λ_s which is a new concept to regulate reverse power flows. A demand charge prevents the customers from simply shifting their on-peak demand to an off-peak period without reducing their peak demand and encourages the customer to reduce their peak demand regardless of the TOU pricing period.

A supply charge addresses the problem of excessive electricity sales to the grid especially during solar peak hours. This rule provides an incentive to the customers to either self-consume PV generation, or to curtail their generation output when it exceeds their load requirements. The supply charge is a new concept motivated by PV export being limited to a fixed fraction of PV capacity in some markets (e.g. Germany), but provides an economic incentive to reduce exports rather than a strict rule. In what follows a *capacity charge* (CC) combines both a demand charge and supply charge.

Without loss of generality, we assume here the supply charge tariff is equal to the demand charge tariff. Then, the customer monthly peak net demand is subject to the CC tariff $\Lambda = \Lambda_s = \Lambda_d$. The CC is based on the peak electricity supplied to the customer or delivered to the grid across a month. That is, the customer's largest absolute net demand over each month is multiplied by the CC tariff Λ in the billing process.

2.2.4 Energy Storage System Model

We constrain the ESS charge/discharge $\boldsymbol{u}$ by $\underline{B}\mathbb{1} \leq \boldsymbol{u} \leq \overline{B}\mathbb{1}$, where $\underline{B}$ and $\overline{B}$ are the discharge and charge power limit of the ESS, respectively.

The state of charge (SOC) is defined by

$$\chi(k) := \chi(0) - \sum_{k=1}^{s} u(k)\Delta t, \tag{2.2}$$

where $\chi(0)$ denotes the initial state of charge.

The rated energy capacity of the ESS is represented by C in kWh. We represent the *minimum allowed SOC* and the *maximum allowed SOC* of the ESS in kWh as $\underline{\mathbf{C}}$ and $\overline{\mathbf{C}}$, where $\underline{\mathbf{C}} := 0$ and $\overline{\mathbf{C}} := C$. Note that $\underline{\mathbf{C}}$ could be set to a fraction of C for a specific energy storage technology that would otherwise degrade when fully discharged. It is assumed here that the efficiency of the ESS is 100% and that degradation is negligible.

We assume each customer has an ESS with an identical storage capacity of 10 kWh and a charging and discharging limit of 5 kW. This is centered within the range of ESS capacities (2-22kWh) considered in other residential ESS studies (Vieira et al., 2017; Luthander et al., 2016; Zhang et al., 2016; Ren et al., 2016b,a; Ranaweera and Midtgård, 2016; Ratnam et al., 2015a). Customer load and PV generation characteristics are provided in Sectoin 2.3.2.

2.2.5 Scheduling Algorithm

We construct a constrained optimization problem to minimize the monthly electricity bill of a customer with an ESS. The customer-owned ESS is dispatched daily solving the following convex optimization problem:sec:CP

$$\min_{\boldsymbol{p}\in\mathbb{R}^s} \Delta t \boldsymbol{\Lambda}_e^T \boldsymbol{p} + \Lambda[\max\{||\boldsymbol{p}||_\infty, p^*\} - p^*], \tag{2.3}$$

such that $\boldsymbol{A}\boldsymbol{u} \leq \boldsymbol{b}$, $\mathbb{1}^T\boldsymbol{p} = 0$, where $\boldsymbol{A} \in \mathbb{R}^{4s\times s}$, $\boldsymbol{b} \in \mathbb{R}^{4s}$, $\boldsymbol{u} \in \mathbb{R}^s$, $\boldsymbol{\Lambda}_e \in \mathbb{R}^s$, $\Lambda \in \mathbb{R}$, $p^* \in \mathbb{R}$. The customer net demand $\boldsymbol{p}$ is defined by Eq. 2.1, where $\boldsymbol{l} \in \mathbb{R}^s$, $\boldsymbol{g} \in \mathbb{R}^s$, $\boldsymbol{c} \in \mathbb{R}^s$, and $k \in \{1,...,s\}$. For configurations a and c, $\boldsymbol{p} \geq 0$. The infinity-norm of $\boldsymbol{p}$ is $||\boldsymbol{p}||_\infty = \max\limits_{1\leq k\leq s} |p_k|$.

We introduce an inequality constraint $\boldsymbol{A}\boldsymbol{u} \leq \boldsymbol{b}$ that represents the ESS charge/discharge and capacity constraints, where $\boldsymbol{A} = \begin{bmatrix} \boldsymbol{I} & -\boldsymbol{I} & -\boldsymbol{T} & \boldsymbol{T} \end{bmatrix}^T \in \mathbb{R}^{4s\times s}$ and $\boldsymbol{b} = \begin{bmatrix} \overline{B}\mathbb{1}^T & \underline{B}\mathbb{1}^T & \underline{\mathbf{C}}\mathbb{1}^T & \overline{\mathbf{C}}\mathbb{1}^T \end{bmatrix}^T \in \mathbb{R}^{4s}$. Each component in $\boldsymbol{A}$ and $\boldsymbol{b}$ was introduced in Section 2.2.1 and 2.2.4.

The equality constraint $\mathbb{1}^T\boldsymbol{p} = 0$ prevents energy-shifting between days. It ensures

that $\chi(s)$, the final SOC at time $s\Delta t$, equals to the initial SOC $\chi(0)$ and hence prevents the ESS from storing extra energy for the following day. Throughout the simulations we set $\chi(0)$ to 50% of the rated energy capacity C, consistent with the approach taken in Ratnam et al. (2015a).

If $||\boldsymbol{p}||_\infty \leq p^*$, then the formulation in Eq. 2.3 is equivalent to the minimization of the linear objective function $\Delta t \boldsymbol{\Lambda}_{\mathrm{e}}^T \boldsymbol{p}$ with the inequality constraint $||\boldsymbol{p}||_\infty \leq p^*$. Otherwise $||\boldsymbol{p}||_\infty$ replaces the existing p^* as the new net demand prediction for the days remaining in the billing period.

Since there is no cost associated with the charge/discharge rate or excessive cycling of the ESS in the objective function, the CO-based scheduling algorithm might charge or discharge the ESS within the same TOU pricing period without any financial benefit to the customer. To eliminate these instances we add a penalty term f_{penalty} to Eq. 2.3 given by

$$f_{\mathrm{penalty}} = 10^{-6}||\boldsymbol{u}||_2 \ , \tag{2.4}$$

where $||\boldsymbol{u}||_2 \in \mathbb{R}^s$ is the Euclidean norm of the ESS charge/discharge schedule. We multiply the Euclidean norm with 10^{-6}\$/kW to make it small compared to the rest of the objective function in Eq. 2.3 and ensure it does not alter the minimum objective function value achieved.

We solve the CO-based scheduling algorithm using MATLAB (Version 2016b) with the convex modeling framework CVX (Version 2.1) and the solver Gurobi (Version 7.0.2).

2.2.6 Operational Inputs

At the start of each day, a day-ahead forecast for solar PV generation and a day-ahead load prediction are required for each customer. Since demand and solar forecast

techniques are not within the focus of this study, the day-ahead forecasts are taken equal to the observed data, i.e. perfect information. With this perfect information we model the upper limit of performance of the CO-based scheduling algorithm as forecast errors typically result in increased demand charges due to premature battery discharge.

In addition, at the beginning of each month a prediction, p^*, is made for the month-ahead customer absolute net demand peak to avoid excessive peak reductions during the first days of the month. The CO-based scheduling algorithm in Eq. 2.3 is used to find the optimal dispatch solution of the ESS for the month-long ($N_{\text{day}} \times s$) data set collected during the previous month. The resulting maximum absolute net demand is used as the prediction, p^*, for the current month.

Net demand prediction is an essential component for economic performance of the CO-based scheduling algorithm but if a simpler implementation was desired, p^* could be set to zero at the beginning of the month.

2.2.7 Customer Billing

The billing period spans a calendar month starting with the first day of each month of the year. The TOU (volumetric) electricity charges, denoted by (EC), for a calendar month are defined by

$$\text{EC} := \sum_{n=1}^{N_{\text{day}}} \Delta t \boldsymbol{\Lambda}_{\text{e}}^T \boldsymbol{p}_n \,, \tag{2.5}$$

where N_{day} is the number of days in the month and $\boldsymbol{p}_n$ is a vector of size s representing the daily net demand profile (e.g., the first day of the month $\boldsymbol{p}_1 = \{p_{1,1}, ..., p_{1,s}\}$).

Peak capacity charges, denoted by CC, are also factored into the monthly bill and are defined by

$$\text{CC} := \Lambda p_{\max} \,, \tag{2.6}$$

where $p_{\max} = \max(||\boldsymbol{p}_1||_\infty, ..., ||\boldsymbol{p}_{N_{\text{day}}}||_\infty)$ is the maximum absolute net demand of the customer observed in the calendar month.

The total monthly electricity bill (i.e., total charge), denoted by TC, is then

$$\text{TC} := \text{EC} + \text{CC}\,. \tag{2.7}$$

2.3 Performance Metrics, Residential Customer Data, and Tariff

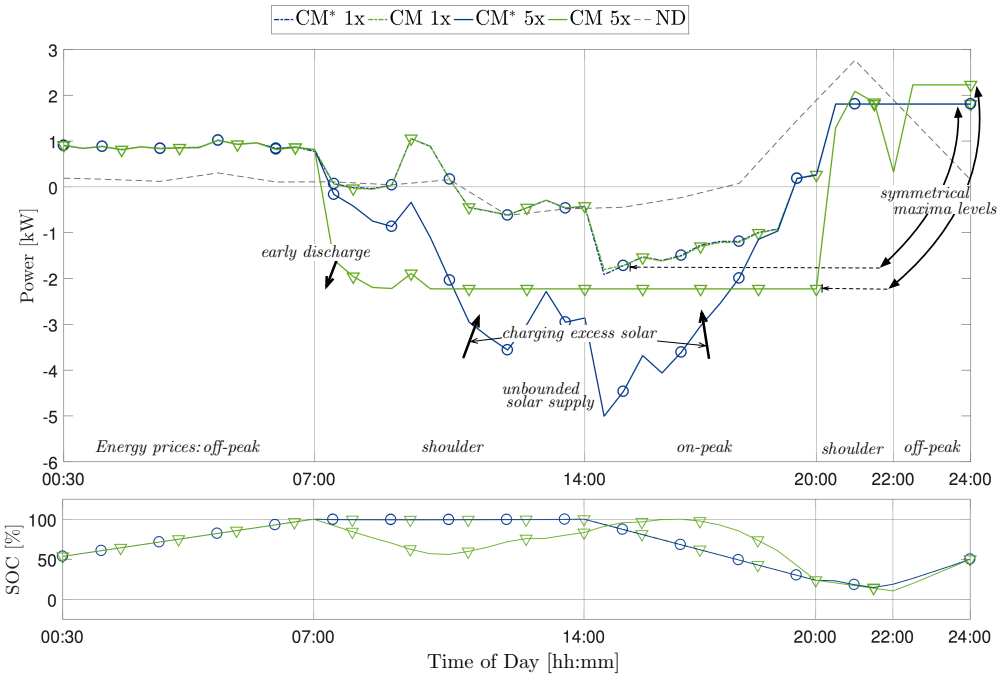

Figure 2.2. Scheduling under increasing solar PV penetration for the customer #38 with configuration *d* (with PV, exports allowed) on October 23, 2011. The customer net demand (with solar PV, but without ESS) is shown as ND and has a peak of 2.76 kW. Each case has a 30-minute resolution and 48 data points in total. To avoid cluttering, the lines are printed with sparser markers that are shown at different points in time. The original solar PV generation data (1x) has been increased by a factor of 5 (5x) to depict increasing PV penetration. The scheduling is done by applying only demand charge, *CM** (blue lines), and a capacity charge that includes a demand charge and a supply charge, *CM* (green lines) as in the rest of the paper.

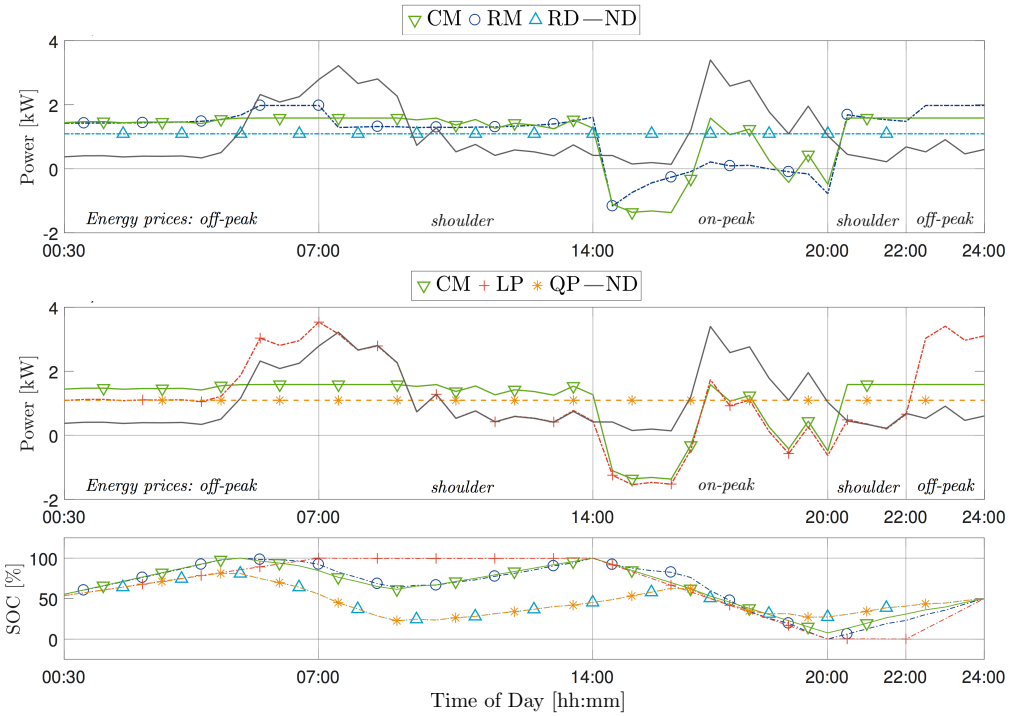

Figure 2.3. Comparison of default case *CM* with the results from reference cases *RM*, *RD* (top) and reference algorithms *LP*, *QP* (middle) for the customer #13 with configuration *b* (no PV, exports allowed) on May 15, 2012. Customer load has a peak of 3.40 kW and a minimum of 0.14 kW. Other cases have the following peak and minimum power in kW: *CM*: 1.59, -1.37; *RM*: 1.98, -1.16; *RD*: 1.09, 1.09; *QP*: 1.09, 1.09; *LP*: 3.53, -1.52.

2.3.1 Performance Metrics

In addition to the reductions in the customer electricity bill defined in Section 2.2.7, we define metrics to quantify how the charge/discharge schedules affect peak demand, PV self-consumption, the net demand profile, and ESS cycling.

Peak Capacity Reduction is the percentage reduction in a customer's peak capacity in a billing month achieved relative to the original net demand without ESS. Peak capacity is defined as the highest 30-minute kW measurement during a billing month.

PV self-consumption is the total amount of solar generation that is consumed locally during the solar hours normalized by the total amount of solar generation. The customers without an ESS consume PV generation insofar as it coincides with their

daytime load. A greater portion of the solar PV generation can be consumed locally by storing generation via an ESS.

Net Demand Fluctuations (NDF) are the sum of the absolute values of differences in adjacent elements of $\boldsymbol{p}$, i.e. fluctuations in the customer net demand profile, normalized by the mean of the absolute net demand, $\overline{||\boldsymbol{p}||}_\infty$.

ESS Cycling is defined as the sum of the absolute values of differences in adjacent elements of $\boldsymbol{u}$, i.e. the number of charge/discharge cycles.

2.3.2 Customer Load and PV Data

We consider publicly available residential PV generation and load data for customers located in distribution networks operated by Ausgrid, an electricity utility in Australia. The data set includes 3 years of separately reported kWh measurements of load and PV generation, beginning 1 July 2010 with 30-minute averaging intervals.

We use a subset of the originally released data set that contains 54 customers with the highest quality data per Ratnam et al. (2015b). The customer IDs of this subset are given in Table 4 of Ratnam et al. (2015b). We further discard Customer 2 as some data recordings of this customer are missing. The average daily energy consumption among these 53 customers is 17.4 kWh with a minimum of 7.0 kWh and a maximum of 35.4 kWh. The average PV system size is 2.5 kW with a minimum of 1.1 kW and a maximum of 10.0 kW. The average daily PV generation is 9.0 kWh with a minimum of 4.2 kWh and a maximum of 39.3 kWh.

2.3.3 Tariff

We consider the residential TOU tariff EA025 (Ausgrid, 2016) in Table 2.1. The TOU tariff does not include a demand charge, so we include the demand charge of the TOU tariff EA302 (Ausgrid, 2016), which is approximately 10.7 AU$/kW-month. Hledik

Table 2.1. Ausgrid Residential TOU tariff (EA025) network energy prices (Ausgrid, 2016). This tariff is effective from 1 July 2016 to 30 June 2017 including goods and services tax in Australia. These energy prices are multiplied with a constant of 0.56 to adjust the original customer electricity bills to the addition of a demand charge to this volumetric energy charge only TOU tariff.

		Energy Prices
Time of Use	Designation	(AU¢/kWh)
Until 7:00	Off-peak	2.7863
7:00 - 14:00	Shoulder	5.4762
14:00 - 20:00	On-Peak	26.4651
20:00 - 22:00	Shoulder	5.4762
Until Midnight	Off-peak	2.7863

(2014) reports that demand charges in the current U.S. tariffs vary between US$1.50/kW-month and US$18.10/kW-month and the EA302 demand charge tariff roughly lies at the mean of this range. The supply charge tariff is set equal to this demand charge tariff.

As we add a demand charge, we subsequently reduce volumetric rates. It would not be realistic to simply add a demand charge to an existing volumetric energy charge only tariff since tariffs with a demand charge often have lower volumetric charges. To avoid overestimating the bill savings we scale down the volumetric charges of EA025 by a constant such that the average customer bill is the same amount as without a demand charge. By means of iterative computation we determined a constant scale factor of 0.56.

2.4 Case Studies and Results

Here we introduce the case studies that benchmark the performance of the CO-based scheduling algorithm and examine the effects of introducing a supply charge to the existing tariff structure. The overview of all case studies is given in Table 2.3.

2.4.1 Default case: Case Monthly (*CM*)

We solve the optimization problem described in Eq. 2.3 over all days in a billing month individually (as opposed to over the whole month at once, consider further RM below). On the first day of each billing month, a net demand prediction, p^*, for the current month is made as described in Section 2.2.6. This net demand prediction is updated when it is exceeded by a daily dispatch solution during that month. We denote this case as *CM* (case monthly).

When *CM* does not include a supply charge, it is denoted as CM^*. For this case $||\boldsymbol{p}||_\infty$ in Eq. 2.3 simplifies to $\boldsymbol{p}$ and Λ in Eq. 2.3 and in Eq. 2.6 becomes Λ_d.

2.4.2 Reference Cases

There are two reference cases considered to assess the economic performance of the CO-based scheduling algorithm namely (1) the customers accurately predict the month-ahead electricity demand and generation, and (2) the customers schedule their ESS without estimating their monthly net demand. These reference cases are structured considering information availability to the customer on historical and future net demand.

RM: Perfect information on monthly net demand

A customer achieves maximum operational savings over a month when TC in Eq. 2.7 is simultaneously minimized over a set of $\boldsymbol{p}_n$ for all days $n \in \{1,...,N_\mathrm{day}\}$. In this reference case we optimize with known customer load and solar PV generation of a whole month ($N_\mathrm{day} \times s$).

While it is not realistic to assume knowledge of monthly customer load and solar PV generation, the solution to this reference case determines the theoretical upper bound on TC achievable by the scheduling algorithm. We denote this reference case as *RM* (reference monthly).

Table 2.2. The objective functions of Linear Program (LP) and Quadratic Program (QP) presented in Ratnam et al. (2015a) along with CO-based scheduling algorithm presented in this work. All algorithms have the same set of constraints as described in Section 2.2.

CO-based Scheduling Algorithm	Linear Program	Quadratic Program$^{\diamond}$
Cost Minimization	Cost Minimization	Power Minimization
$\min_{\boldsymbol{p}\in\mathbb{R}^s} \Delta t \boldsymbol{\Lambda}_{\mathrm{e}}^T \boldsymbol{p} + \Lambda[\max\{\|\|\boldsymbol{p}\|\|_\infty, p^*\} - p^*]$	$\min_{\boldsymbol{p}\in\mathbb{R}^s} \Delta t \boldsymbol{\Lambda}_{\mathrm{e}}^T \boldsymbol{p}$	$\min_{\boldsymbol{p}\in\mathbb{R}^s} \boldsymbol{p}^T \mathbf{I}\, \boldsymbol{p}$

$^{\diamond}$The matrix $\boldsymbol{H}$ in QP, originally defined as $\boldsymbol{H} \in \mathbb{R}^{2s\times 2s}$, is simplified here as $\boldsymbol{H} := \mathbf{I} \in \mathbb{R}^{s\times s}$.

RD: Daily Scheduling without p^*

When the daily scheduling solution is determined without a net demand prediction, i.e. $p^* = 0$, the scheduling algorithm overvalues the capacity charge reduction. The resulting scheduling does not necessarily achieve the best economic operation since the daily reduction of the capacity charge is unnecessary when the net demand of a day does not exceed the preexisting maximum net demand.

In this reference case p^* is set to zero for each day of the month and the results give the lower theoretical bound on EC achievable by the scheduling algorithm. We denote this reference case as *RD* (reference daily).

2.4.3 Reference Algorithms

The CO-based scheduling algorithm is compared against two alternate approaches to designing day-ahead charge/discharge schedules. Two approaches, namely QP-based energy shifting and LP-based energy shifting have been presented in Ratnam et al. (2015a), and will serve as reference cases. The objective functions used in both methods are given in Table 2.2. The constraints described in Section 2.2 also apply for both methods.

LP: Best EC Minimization

The Linear Program maximizes the operational daily EC savings by energy shifting and/or energy arbitrage. When the customer cannot sell energy back to the grid, this method minimizes the operational costs by shifting energy use of the customer from on-peak pricing periods to off-peak pricing periods. When energy arbitrage is allowed, the net demand profile of the customer becomes irrelevant for ESS scheduling and the method instead focuses on maximizing the profit from arbitrage.

This method dispatches ESS in the most profitable way possible when the customer is not subject to a demand or a supply charge tariff. Thus it determines the upper performance bound for the EC minimization using ESS. We solve this optimization problem using MATLAB (Version 2016b) with the convex modeling framework CVX (Version 2.1) and the solver Gurobi (Version 7.0.2). We denote this reference method as *LP*.

QP: Mitigation of Power Fluctuations

The Quadratic Program minimizes the daily fluctuations in the net demand profile of the customer through energy shifting while also reducing peak net demand. QP ignores the TOU rate structure. As a consequence, it does not necessarily improve the operational savings of the customer. This method depicts a grid-friendly ESS operation mode and represents the performance bound in that context. We solve this optimization problem using MATLAB's *interior-point-convex quadprog* algorithm. We denote this reference method as *QP*.

2.4.4 Example CO-based algorithm schedule

An example charge schedule is given in Figure 2.2 for *CM* (green lines) and *CM** (blue lines). In this case the customer has a 1.05 kW solar PV system and can send back

Table 2.3. An overview of the case studies. Plus (+) indicates that monthly net demand p^* is predicted for the customer. This prediction is set to 0 for *RM* and *RD*. Minus (−) indicates cases that do not consider demand charges in their formulation and thus do not require a net demand prediction. The acronyms of the case studies (Section 2.4) stand for *case monthly* (*CM*), modified *case monthly* (*CM**), *reference monthly* (*RM*), *reference daily* (*RD*), *linear program* (*LP*), *quadratic program* (*QP*).

Case	Method	p^*	Description
CM	CO	+	Default case.
CM*	CO	+	Default case without considering a supply charge.
RM	CO	+	Best theoretical economic performance achievable by CM.[†]
RD	CO	0	Reference case that minimizes daily (rather than monthly) capacity charge.
LP	LP	-	Best economic performance without a demand or supply charge tariff.
QP	QP	-	Best mitigation of power fluctuations in a net demand profile.

[†]We assume knowledge of month-ahead customer data to construct an upper performance bound for *CM*.

energy to the grid (configuration *d*). To demonstrate the characteristic behavior of the scheduling algorithm under increasing PV penetration, we increase the solar PV system size of the customer. We designate the customer with the original solar PV generation as 1x (dashed lines) and increase this generation by a factor of 5 (solid lines) denoted as 5x.

In all cases, the scheduling algorithm shifts customer load away from the on-peak pricing period and charges the ESS during the off-peak pricing periods while capping the net demand peak. Since *CM** does not consider a supply charge tariff the solar generation is simply fed to the grid. The ESS is instead charged during the off-peak pricing period before 7:00 of the day until it is fully charged and then discharged during the on-peak pricing period to maximize cost reductions.

CM follows the same scheduling in the 1x case with a single deviation in scheduling at 14:30 of the day when it restricts the maximum supply to the same level of the maximum demand to avoid an increase in the customer's peak capacity. We observe a significant change in scheduling pattern for the 5x case. The ESS is being discharged

starting at 7:00 of the day in preparation for absorbing excess generation at solar peak hours and cap the maximum supply to the same level of the maximum demand. Nevertheless, the scheduling algorithm is still forced to increase the peak capacity of the customer by 23% in this case.

Table 2.4. Details of scheduling under increasing solar PV penetration for the customer #38 on October 23, 2011. *Max. Supply* is the maximum power that the customer supplies to the grid. *Daily EC* shows the daily energy cost of the customer. A negative value of *Daily EC* indicates a financial compensation to the customer. The values given in parentheses show results for the same customer without an ESS.

Demand Charge (CM)*	Max. Demand [kW]	Max. Supply [kW]	Daily EC [AU$]	PV Self-consumption [%]
PV Penetration				
1x	1.81 (2.76)	1.92 (0.63)	-1.64 (0.60)	57.8 (49.8)
2x	1.81 (2.76)	2.67 (1.40)	-2.54 (0.60)	34.2 (31.1)
5x	1.81 (2.76)	5.01 (3.73)	-5.22 (0.60)	15.8 (14.9)
Capacity Charge (CM)	Max. Demand [kW]	Max. Supply [kW]	Daily EC [AU$]	PV Self-consumption [%]
PV Penetration				
1x	1.81 (2.76)	1.81 (0.63)	-1.64 (0.60)	57.9 (49.8)
2x	1.81 (2.76)	1.81 (1.40)	-2.54 (0.60)	34.1 (31.1)
5x	2.23 (2.76)	2.23 (3.73)	-4.82 (0.60)	30.0 (14.9)

Table 2.4 shows how the maximum demand, the maximum supply, the energy cost to the customer and the PV self-consumption change with increased PV penetration levels. In addition to the cases in Figure 2.2, we also present results for the 2x case where the solar generation of the customer is increased by a factor of 2. The customer's energy cost is not impacted by the introduction of a supply charge in the 2x case and the ESS cycling does not change. The compensation to the customer is reduced roughly by 8% in the 5x case but the customer's maximum energy supply is also significantly reduced from 3.73 kW to 2.23 kW. The ESS approximately makes one additional cycling for this case. The PV self-consumption stays similar for the 1x and 2x cases but it is increased by more than %14 with the introduction of a supply charge.

2.4.5 Example scheduling for all case studies

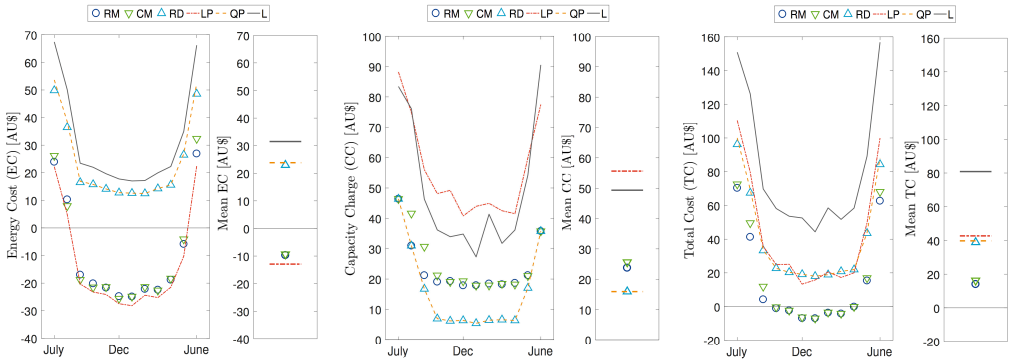

Figure 2.4. Electricity cost breakdown of all scheduling cases for the customer #13 with configuration *b* (no PV, exports allowed) covering a 2-year data set. The costs for the original customer load is shown as L. Scheduling is optimized during each billing month. The average (of the two) values for each billing month are shown. The annual mean for each case is shown to the right of each figure. Note that the June is Winter in the Southern hemisphere.

Here we present representative results for one day. In this case the customer can send back energy to the grid but does not have a solar PV system (configuration *b*). The customer has an average daily load of 12.3 kWh with a minimum of 1.6 kWh and a maximum of 64.8 kWh. Figure 2.3 shows the net demand profiles and the SOC optimized under each case study excluding *CM**. All charge schedules start the day with charging the ESS in the off-peak period. *LP* purchases and stores off-peak energy until the storage is full, and discharges at the peak period to maximize operational savings while other case studies cycle the ESS during the day in order to reduce peak net demand. All cases charge after 22:00 to fulfill the SOC requirement at the end of the day.

There are three important observations in Figure 2.3: (1) *RD* results in the same charge schedule as *QP* even though *QP* does not consider a TOU tariff in its formulation. *RD* lacks a net demand prediction p^* and consequently it overvalues the peak reduction and flattens the net demand profile in the same way as *QP*. (2) *CM* reduces peak net demand more compared to *RM* for this particular day (see 06:00 - 07:00). However,

when the billing month is considered this lower level of peak net demand is suboptimal with respect to the TC to the customer. Since *CM* does not have the same information as *RM* it optimizes the scheduling for this day with a lower bound on peak net demand. Consequently, *CM* looses flexibility associated with a higher bound on peak net demand which results in economically undesirable discharging during the off peak period (06:00 - 07:00). (3) *LP* practically shifts the original peak net demand to the off-peak period without any mitigation of the peak net demand. It even causes a slight increase in peak net demand of the day by 4%.

In Figure 2.4, the electricity cost breakdown for the same case study (customer #13 and configuration *b*) is shown for the 2-year data set. *LP* marks the lowest bound on EC but *RM* follows this bound very closely. This indicates that the CO-based scheduling algorithm results in charge schedules that perform near-optimally in EC reductions. Furthermore *CM* yields similar results to *RM* even without the same informational leverage that *RM* has. This indicates that given an accurate daily load and solar forecast, and peak net demand predictions based on the previous month, the CO-based schedules can in fact yield near optimal EC reductions for customers in real world ESS operations. Lastly, capacity charges are minimized by QP and RD, while LP performs worst. For the total cost *RM* and *CM* perform best.

2.4.6 Bulk Simulation Results

Using the Ausgrid data (Section 2.3.2) for each customer we perform the optimization with the case studies *CM*, *RM*, *RD*, *QP*, and *LP* for a 2-year period starting in July 2011. The last month of the first year has to be used for the net demand prediction for the first month of the second year in *CM*. Therefore, we do not perform the optimization for the first year data set.

Figures 2.5 - 2.9 present the performance metric results for the bulk simulations.

For each customer 24 metrics calculated for 24 billing months are averaged. The histograms show the distributions of the averaged value for 53 customers.

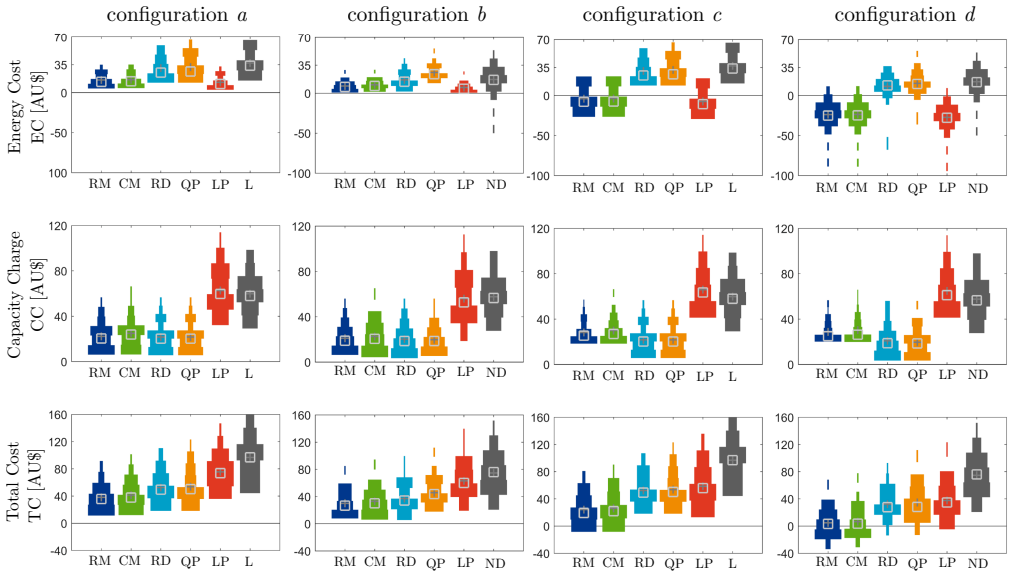

Figure 2.5. Electricity cost breakdown of all scheduling cases for 53 residential customers over a 2-year data set. The columns represent the different configurations given in Figure 2.1. The original customer data is labeled as *L* (load) when a solar PV system does not exist and labeled as *ND* (net demand) otherwise. 24 electricity cost values optimized for 24 billing months are averaged. Then a histogram is drawn for 53 customers. The variation in box plot thickness represents the distribution of the values. Thicker regions mean more customers fall in this bracket. A light colored square sign (□) indicates the median and a dark colored plus sign (+) shows the mean of all customers. A negative cost indicates compensation to the customer.

Electricity Cost

Figure 2.5 gives the EC, the CC, and the TC for each customer system configuration. Overall the results are consistent with those observed for customer #13 in Figure 2.4, but they also highlight some differences between the configurations with and without grid exports. *LP* yields greater reductions in EC in configurations *a* and *b*, where energy sale back to the grid is not incentivized. *RM* and *CM* perform similarly as *LP* and perform especially close to *LP* when energy arbitrage is allowed (configuration *b* and

d). Scheduling through *QP* results in the lowest CC (with RD a close second) since it focuses on flattening the net demand profile. *RM* and *CM* also incur comparably small CC especially when energy sale back to the grid is not incentivized. These observations are in agreement with our earlier observations in Section 2.4.5.

Peak Reduction

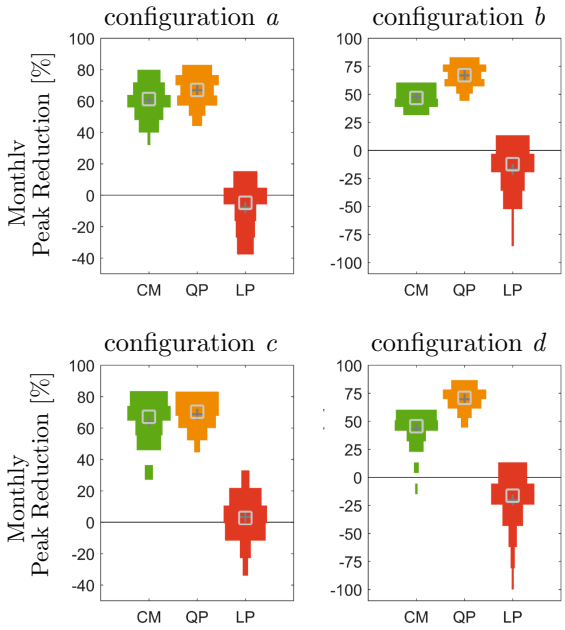

Figure 2.6. Monthly Peak Reductions achieved by *CM*, *QP*, *LP* by configuration. Negative values indicate an increase in peak demand (primarily occuring for *LP*).

Reducing peak demands generally goes along with reduced grid impacts as the infrastructure is utilized more evenly. Figure 2.6 shows peak reductions achieved by *CM*, *QP*, and *LP*. For this figure and the following ones, we only report results for *CM*, *QP*, and *LP* as *RM* and *RD* do not show much difference from *CM* and *QP*, respectively.

QP results in the greatest reductions in peak net demand averaging 67 to 69%, depending on the configuration. *CM* achieves comparable results in configurations *a* and *c* (61%, 64%, respectively) but in configuration *b* and *d* results in lesser peak net demand reductions (51%, 43%, respectively) in return for profit through energy arbitrage in the

top row of Figure 2.5. *LP* is ineffective in peak net demand mitigation and causes an increase in peak net demand for most customers.

Storage Cycling

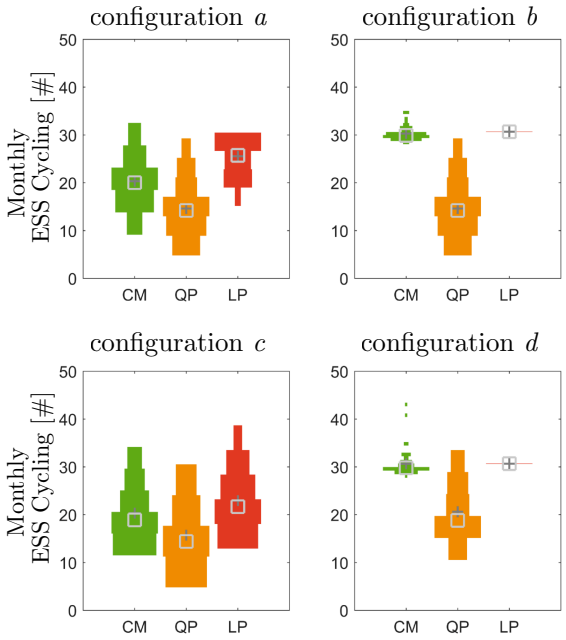

Figure 2.7. Monthly ESS cycling in *CM*, *QP*, *LP* by configuration.

Increased storage cycles go along with a reduction in ESS lifetime. *QP* is the least straining on the ESS in terms of storage cycling in all configurations. For configuration *b*, *CM* and *LP* cause a doubling in cycling due to energy arbitrage. In configuration *b* and *d* with grid exports allowed, *LP* results in a single storage cycle per day for all customers and months; in these cases LP profit is maximized by charging to 100% during the morning off-peak, discharging to 0% on-peak, and charging back up to 50% during the evening off-peak. Since CM similarly utilizes only about one cycle per day in configurations b and d indicates that either (i) customer peak demands coincide with the on-peak period, so a discharging will accomplish both EC and CC objectives or (ii) the energy required to reduce peak demand is small compared to the battery energy capacity.

The cycling for CM may increase compared to LP if smaller batteries were considered.

Net Demand Fluctuation

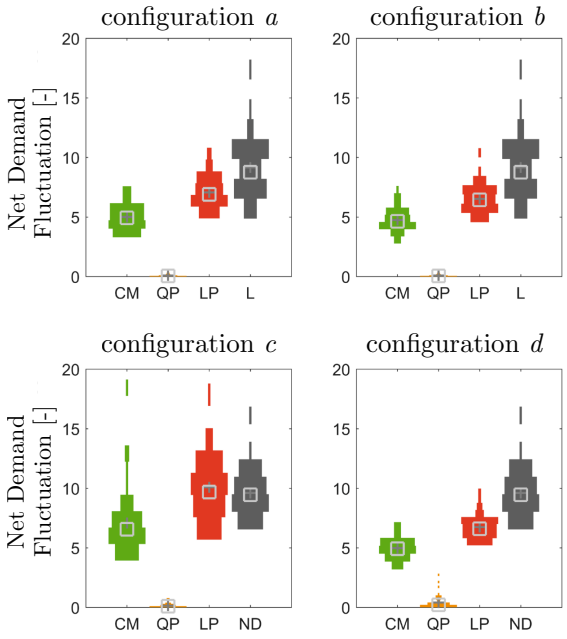

Figure 2.8. Net Demand Fluctuation for *CM*, *QP*, *LP* by configuration in comparison with the original customer data (*L* or *ND*).

Figure 2.8 shows fluctuations in net demand profiles for each configuration and without an ESS. *QP* mostly achieves constant power (flat) customer net demand profiles and reduces net demand fluctuation dramatically. This indicates that the battery is sized large in comparison to most customers' daily load variations. *CM* results in 25 to 50% reductions in net demand fluctuations when compared to the original customer data, while *LP* increases fluctuations by 13% for configuration *c* and yields reductions between 25 - 31% for others.

PV Self-Consumption

Figure 2.9 shows PV self-consumption for each configuration and without an ESS. All cases result in increased PV self-consumption when energy sale back is not

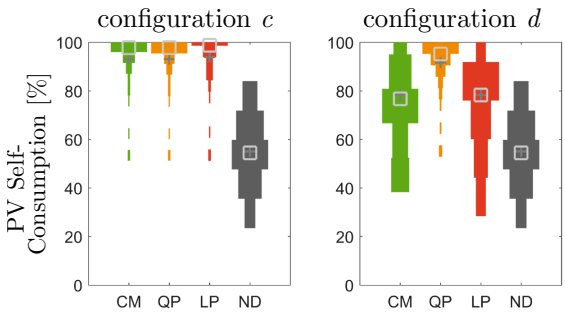

Figure 2.9. PV self-consumption achieved for *CM*, *QP*, *LP* by configuration given along with direct PV self-consumption by the customer (*ND*) without an ESS.

incentivized. *QP* overall results in the largest mean self-consumption with 89 - 93%. *CM*, *QP*, and *LP* achieve the same mean self-consumption in configuration *c* with 93%, a substantial increase over 54% achieved without an ESS. When energy arbitrage is allowed *CM* and *LP* yield lower self-consumptions but still 20% higher than the self-consumption without an ESS.

2.4.7 Impact of a Supply Charge on Solar Supply

In this work we introduced a supply charge tariff that incentivizes ESS customers to store excess solar PV generation that would otherwise result in reverse power flow in the distribution grid. We compare *CM* with *CM** that does not consider a supply charge but still considers a demand charge.

In order to compare performance of *CM* and *CM**, similar to the practice in Figure 2.2, we designate the customer with the original solar PV generation as 1x and increase this generation by a factor of 2. Here we only consider configuration *d* since configuration *a* and *c* do not have solar PV systems, and the constraint $\boldsymbol{p} \geq 0$ in configuration *b* avoids any energy to be supplied back to the grid, thus causes no difference in solar supply with increased PV penetration.

Figure 2.10 shows PV self-consumption, maximum supply to the grid, storage cycling and total cost to the customer achieved in *CM* and *CM**. As the customers

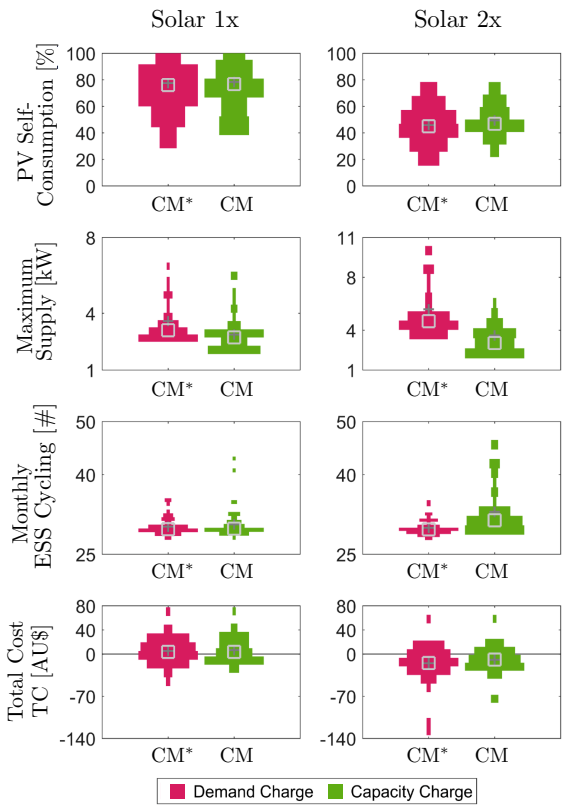

Figure 2.10. PV self-consumption, maximum solar supply to the grid, and total electricity cost under a capacity charge case (*CM*) and a demand charge only case (*CM**). The original solar PV generation (1x) has been increased by a factor of 2 (2x) to investigate sensitivities. Maximum supply is determined by taking the highest amount of supply that the customer provided over the course of 2 years. A negative cost indicates compensation to the customer.

have larger solar PV systems the overall PV self-consumption decreases and the overall maximum supply to the grid increases in both cases. The maximum supply in Figure 2.10 reflects the capacity requirements of the infrastructure that would be required to support the PV system owners.

CM yields higher PV self-consumption than *CM** by 2% and 10% in the 1x case and the 2x case, respectively. Furthermore, it reduces the maximum reverse power flow to the grid in the 2x case by 0.60 kW on average from 4.2 kW without an ESS. The 1x case does not have enough solar PV feed-in (2.0 kW on average) to exceed the peak capacity

of the customers and the maximum reverse power flow does not get penalized by a supply charge in most cases. It results in an increased ESS cycling by 3 cycles per month in the 2x case but causes approximately the same ESS cycling in the 1x case. Moreover, introduction of a supply charge has negligible impact on the customer TC. However, there are a few customers – presumably those with large PV systems – that need to cycle the battery significantly more per month under *CM* with up to 48 cycles. Presumably some of the same customers with the largest PV systems see their TC reimbursements from the utility cut significantly, from up to 140 AU$/month to less than 70 AU$/month.

2.5 Conclusions

We have presented a CO-based charge/discharge scheduling algorithm for distributed ESSs with co-located solar PV systems. The results of a case study including 53 residential customers located in an Australian distribution network confirmed that the daily CO-based charge/discharge schedules reduce (1) peak net demand of the customer (by design), (2) power fluctuations in the net demand profile (ancillary benefit), and (3) the reliance of the customer on the grid by way of promoting energy self-consumption of local solar PV generation (also an ancillary benefit).

We benchmark the performance of the CO-based scheduling algorithm with two alternate methods for behind-the-meter ESS scheduling. Results for 2-years of customer data show that the CO-based scheduling algorithm provides mean monthly peak net demand reductions between 46 - 64%, reduces net demand fluctuations by 25 - 49% on average, and increases the mean solar PV self-consumption between 24 - 39% when compared to the original customer data. Maybe most importantly, the CO-based schedules yield a nearly optimal energy cost reductions.

Prior to deployment of this scheduling algorithm in real-world applications, further work is needed to show susceptibility of the algorithm to load and solar forecast

accuracy as well as ESS sizing (specifically smaller ESS) and inclusion of ESS degradation costs. For specific applications the tariffs should obviously be adjusted to the local conditions.

In this work we have also introduced the concept of having a supply charge in electricity rates. We demonstrated that introduction of a supply charge does not financially impact customers with an ESS while it encourages customers to reduce their peak solar power supply to the grid. This new tariff mechanism reduces the maximum monthly solar PV power supply to the grid by 19% on average in the data set considered here.

We envision our assessment would assist policy makers in developing tariff structures where a penalty or subsidy on restricting solar power supply may encourage customers to reduce reverse power flow through procurement of ESSs. This, in return, would help utilities to support more distributed renewable energy generation on their distribution systems.

The text and data in Chapter 2, in full, is submitted for publication of the material with the title "Distributed energy storage system scheduling considering tariff structure, energy arbitrage and solar PV penetration". Babacan, Oytun; Ratnam, Elizabeth L.; Disfani, Vahid R.; Kleissl, Jan. The dissertation author is the primary investigator and author of this article.

Chapter 3

Effects of Residential Electricity Storage on Electric Power Emissions in the U.S.

3.1 Introduction

Decarbonization of the electric power sector cannot be achieved by reducing system demand only. Electricity consumed at different times of the day and year has different underlying resource costs and emissions impact (Jamasb and Pollitt, 2011). In this regard, energy storage could play an important role in reducing overall operation costs and emissions by offering operational flexibility in the power system while providing reserve capacity to markets (de Sisternes et al., 2016). Energy storage is often considered as an essential component of the future electric grid for widespread use of wind and solar technologies (de Sisternes et al., 2016; DiOrio et al., 2015).

Energy storage is often assumed to reduce pollutant emissions to the environment with low or no direction emissions during its operation. However, numerous studies argue that adding energy storage to the electric power sector is not necessarily a low pollution solution. Hittinger and Azevedo (2015); Carson and Novan (2013) show that the operation of energy storage can increase overall emissions when arbitraging wholesale prices during peak and non-peak hours. During this type of operation, the storage shifts

electricity consumption across time and place, thereby leveling out the system load. This, in return, might potentially defer investments in other more expensive generation assets. However, there is a strong incentive for such large, energy-intensive applications to use electricity at night rather than during the day when most of the electricity is usually generated by conventional fossil fueled power plants, often a coal plant (Hittinger and Azevedo, 2015; Jamasb and Pollitt, 2011). As a result, whether the ongoing deployment of grid-connected energy storage would be successful in helping reaching future emission constraints greatly depends on how storage would be operated.

It is not clear yet how customer-owned energy storage systems should be regulated. Nevertheless there is a growing market for residential energy storage. The deployment of non-hydro energy storage systems is expected to grow at an unprecedented rate in the coming decade. IFC (2017) predicts an annual deployment in emerging markets worldwide (outside Western Europe, U.S., and Japan) of 10 GW by 2021. GTM Research and ESA (2017) forecast that energy storage deployment in 2021 will exceed 2 GW annually in the U.S. whereas it was only around 0.2 GW in 2015. Nearly half of these deployments are predicted to happen in non-utility energy storage systems. BNEF (2017) expects total behind-the-meter energy storage to rise from around 0.4 GWh today to nearly 760 GWh in 2040.

It is crucial to understand the potential impact that residential storage will bring to the system. It would be a fair assumption that residential customers would most likely operate their storage systems for reducing their electricity costs. Electric utilities usually offer tariffs that has fixed energy use charges, in part, to protect the end-users from the price volatility that occurs during peak demand hours. Utilities also offer time of use pricing that allows voluntary users to respond to the peak demand hours by reducing their demand and in return provides them reduced energy charges during off-peak hours. Fixed charge tariff structures are not financially beneficial for storage owners since it does not

allow arbitraging but they could exploit the time of use pricing in order to reduce their electricity bills. In this work, we investigate the net emissions resulting from economic operation of residential energy storage.

3.2 Methods and Data

3.2.1 Customer System Configurations

We consider three types of residential customer: (1) A customer without a solar PV system or ESS; (2) a customer who owns a behind-the-meter ESS; and (3) a customer who owns a behind-the-meter ESS co-located with a solar PV system.

The base customer (#1) is assumed to be under a tiered rate plan. This rate plan has fixed pricing levels, known as "tiers". The customer has a monthly baseline allowance where electricity has a relatively low price. Additional prices apply if the customer exceeds their baseline allowance. This is the benchmark customer.

The customer who owns a behind-the-meter ESS (#2) is assumed to enrolled in a time-of-use tariff. The peak and off-peak pricing periods of this plan allows this customer to reduce its monthly electricity bill through energy shifting. We do not consider a net metering for the customer, thus ESS cannot be discharged for energy sale back to the grid. This customer configuration is shown as configuration *a* in Figure 2.1.

The customer who has both a behind-the-meter ESS and a solar PV system (#3) is similarly enrolled in a time-of-use tariff. For this customer, we investigate two cases: (1) the customer is not enrolled in a net metering program and has to self-consume or curtail the solar PV generation, and (2) the customer is enrolled in a net metering program and compensated at the full retail rate of the electricity. These cases are shown as configuration *d* in Figure 2.1, respectively.

3.2.2 Customer Load and Solar Data

We consider publicly available residential load profiles covering numerous locations in the U.S. provided by Open Energy Information (Open Energy Information, 2014). These data sets are created using a reference case house model representing a house built to the 2009 International Energy Conservation Code (IECC), as well as considering several other standards related to domestic appliances, lighting and miscellaneous electric loads (Hendron and Engebrecht, 2010). The representative electrical load for this benchmark house is reported for the typical meteorological year version 3 (TMY3) station locations using the weather files available for each selected TMY3 stations. TMY3 data sets (National Solar Radiation Data Base, 2015) provides annual data set that holds hourly meteorological values that typify conditions at a weather station over 14 - 30 years (Wilcox and Marion, 2008).

The expected power output for each TMY3 site is calculated using the TMY3 data and a PV performance model presented in Jamaly et al. (2013). This model considers irradiation, wind speed and ambient air temperature data and calculates the AC performance output of a PV system.

3.2.3 Marginal Emissions Factors

The emissions due to electricity generation vary with many factors. The type of power plants activated to supply the marginal amount of energy needed changes with location and time. Thus the emissions reduction achieved by a demand-side intervention in the electricity system is typically assessed by a rate, which measures the emission intensity of electricity not used as a result of the intervention (Hawkes, 2010). In other words, this rate is the emissions intensities of the last generator that is needed to meet demand at a given time. This emissions rate is defined as the marginal emissions factor (MEF).

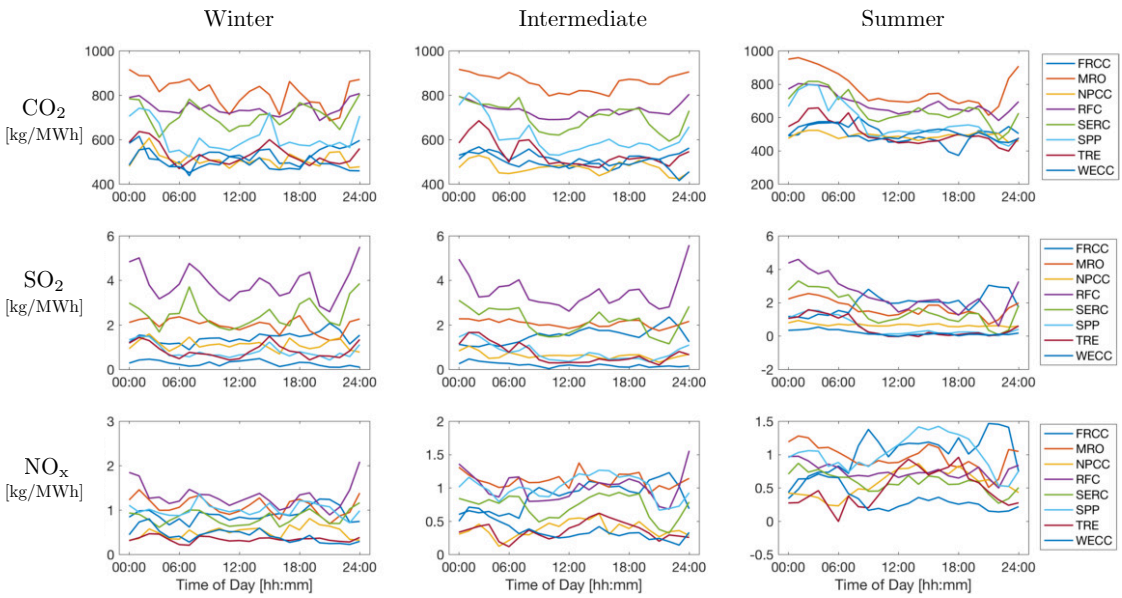

Figure 3.1. Time-of-day trends of MEF estimates by season reported by Siler-Evans et al. (2012). Summer months are May through August; winter months are December through February; and remaining intermediate months are March, April, September and November.

There are a range of methods for estimating MEFs. A merit order based energy models (e.g. Voorspools and D'haeseleer (2000); Bettle et al. (2006)) simulate unit-by-unit dispatch and attempt to model the operational decisions made by controllers and grid operators. Other methods (e.g. Hawkes (2010); Siler-Evans et al. (2012)) rely on historical operating data and couples historical hourly generation and emissions of resources to determine hourly marginal rates. The advantage of this approach over a merit order based model is that MEFs can be systematically calculated over a large geographic region without a necessity to model detailed transmission, generator, and reliability constraints.

In this work we utilize MEF reported by Siler-Evans et al. (2012) for each North America Electric Reliability Corporation (NERC) region. The regional MEFs are determined using regressions of hourly generation and emissions data from 2006 through 2011. The data set contains seasonal MEF trends by time-of-day for CO_2, SO_2, and NO_x

emissions as shown in Figure 3.1.

One limitation of these MEF estimates is that they do not account for biomass, wind, nuclear, hydropower, waste-to-power, geothermal, solar, and small fossil-fueled generators. Only fossil-fueled generators greater than 25MW is accounted. Thus these estimates would be only valid if only these large fossil-fueled generators operate as the marginal generator. This is a reasonable assumption since renewable resources, hydropower and nuclear usually do not respond to the marginal changes in demand. Furthermore, Siler-Evans et al. (2012) report the share of small fossil-fueled generators in each region that is not accounted for. The majority consists of combined heat and power (CHP) generators that are unlikely to affect the MEF estimates (Marnay et al., 2002). Finally, non-CHP generators that act as a marginal generator comprise only less than 3% of the total generation capacity.

3.2.4 Utility Sampling and Tariff

Electricity is supplied to the majority of the consumers in the U.S. by investor-owned or publicly-owned utilities. Each utility has exclusive franchises to sell electricity to the retail consumers in their areas at prices approved by state regulatory commissions (Neeland, 2009). To account for a larger consumer population we consider the biggest utility by the customer size in each NERC region as reported in U.S. Energy Information Administration (2016). On exception is in Southwest Power Pool (SPP). Here we choose the second biggest utility Westar Energy instead of Oklahoma Gas & Electric since it offers a residential demand charge, which is a rare tariff structure to find in current rate offerings. In addition to this list we consider two additional utilities: Southern California Edison and Virginia Electric & Power. Southern California Edison is chosen to compare two utilities serving in the same state. Virginia Electric & Power is chosen to compare two utilities serving in the same NERC region that also offers a residential demand

Table 3.1. The list of utilities under consideration and the number of customers they serve as reported in (U.S. Energy Information Administration, 2016). NERC Regions are Florida Reliability Coordinating Council (FRCC), Midwest Reliability Organization (MRO), Northeast Power Coordinating Council (NPCC), ReliabilityFirst Corporation (RFC), SERC Reliability Corporation (SERC), Southwest Power Pool, RE (SPP), Texas Reliability Entity (TRE),Western Electricity Coordinating Council (WECC). The time of use tariffs (TOU) offered by each utility is also given. A TOU that only includes a volumetric charge denoted as eTOU (energy TOU). A TOU that consists of a volumetric charge and a demand charge is denoted as dTOU (demand TOU). The tariff survey is completed in May 2017 and this list includes tariffs in effect at that time. "-" indicates unavailability of a tariff structure.

Entity	State	NERC	Customer Size	eTOU	dTOU
Florida Power & Light	FL	FRCC	4,708,793	+	-
Consumers Energy	MI	MRO	1,796,196	+	-
Consolidated Edison Co-NY	NY	NPCC	2,545,762	+	-
DTE Electric Company	MI	RFC	2,153,990	+	-
Georgia Power Co	GA	SERC	2,439,237	+	+
Virginia Electric & Power	VA	SERC	2,405,875	+	+
Westar Energy	KS	SPP	375,809	+	+
TXU Energy Retail	TX	TRE	1,667,703	+	-
Pacific Gas & Electric	CA	WECC	5,069,189	+	-
Southern California Edison	CA	WECC	4,990,840	+	-

charge. The complete list of the utilities under consideration is given in Table 3.1.

3.2.5 Simulation Setup and ESS Scheduling

For each utility in Table 3.1 we locate TYM3 stations that fall under each utilities service territory. The California TMY3 station coverage is given in Figure **??** as an example. We identified varying numbers of TYM3 stations for each utility ranging from 4 (Consolidated Edison Co-NY) to 31 (Virginia Electric & Power). On average 17 stations all under each utility service territory. Consolidated Edison Co-NY is an outlier since it only serves New York City and a neighboring county, which is considerably small territory compared to geographic areas other utilities are serving.

We use the constrained optimization problem presented in Section 2.2.5 to min-

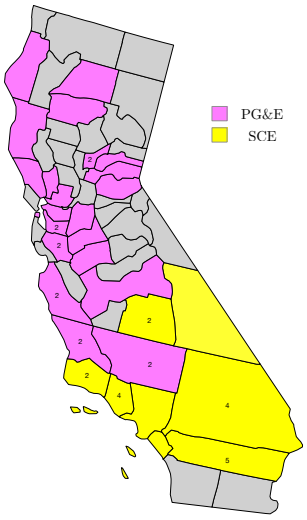

Figure 3.2. The coverage of TMY3 stations by the service territory of Pacific Gas & Electric (PG&E) and Southern California Edison (SCE) utilities in California. The boundaries indicate county lines in California. Some counties have multiple TMY3 stations in their area.

imize the monthly electricity bill of a customer with an ESS. For tariff structures that only include a volumetric charge, denoted as eTOU, we discard the second term in the objective function of Eq. 2.3. If the tariff structure includes a demand charge as well, we use the formulation of Eq. 2.3 as originally presented. We denote this tariff structure as dTOU.

For each customer system configuration described in Section 3.2.1, we get the hourly kW demand as reported in (Open Energy Information, 2014) and compute hourly kW solar generation as described in Section 3.2.2. Throughout our simulations we only consider the case study *RM* that is explained in Section 2.4.2. In this case, a customer achieves maximum operational savings over a month. We assume that the ESS round-trip efficiency is 100% and there is no degradation.

Once we determine the daily charge and discharge schedules, we calculate the

electricity bill according to the tariff under consideration. We also determine the emissions by the customer-owned ESS operation through multiplying the resulting net demand profile with the MEF estimates. We then calculate the cost reductions achieved and the emissions increase or reduction yielded by the ESS operation by comparing the case against the base customer (Section 3.2.1) that does not have a solar PV system or ESS.

3.3 Results and Discussions

We simulate ESS charge and discharge schedules for the three customer configurations described in Section 3.2.1 for all TMY3 stations that are covered by the utilities listed in Table 3.1. In Figure 3.3 we present the results in California for the customer type #2 with configuration *a* that adopts ESS and does not enroll in net metering.

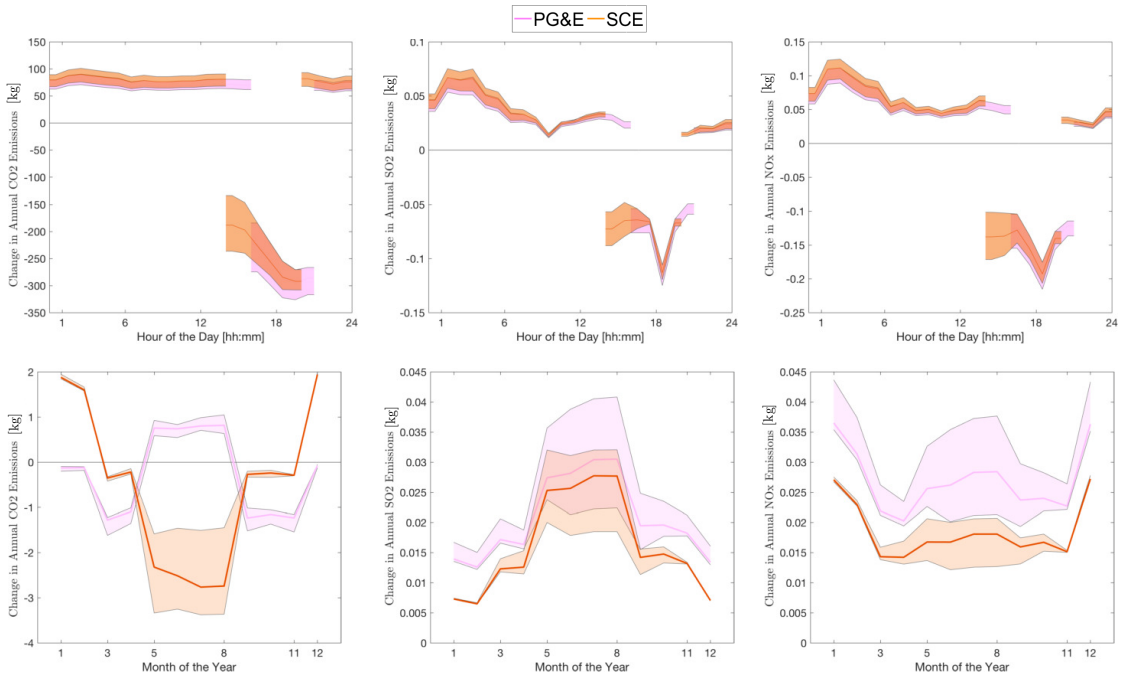

Figure 3.3. The average CO_2, SO_2, NO_x emission impact of the ESS schedules throughout the year categorized by hour of the day (top) and by month of the year (bottom) for the customer type #2 with configuration *a*. The shaded band represents the variation between different customers served by the same utility. The mean of the customers are given by the thick line within the band.

Since PG&E and SCE have different time-of-use periods for their customers (2-8pm and 4-9pm, respectively), the ESS schedules differ considerably. PG&E customers charge their ESS for a longer time period and at a lower charge rate, while SCE customers charge at a higher rate in a shorter period. The band is wider for SCE customers since there is significant difference where the customer are located. Some of the customers are located in hot-dry climates and they have higher electricity loads in the summer months for cooling. Others are located at coastal regions of California where they do not require much air conditioning in their houses.

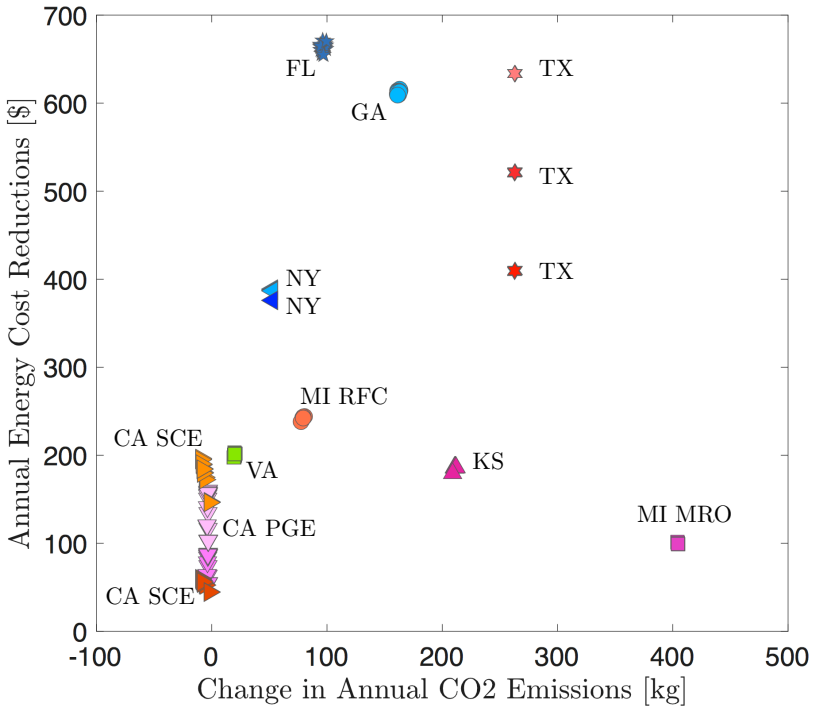

Figure 3.4. The change in annual CO_2 emission and the annual energy cost reductions averaged over all customers in each utility service area. (Customer #2, configuration *a*, that is, ESS only) Each utility is labeled with the state abbreviations. Multiple TOU tariffs are considered or the utilities in Texas, New York and California. Therefore, these states have multiple labels. Michigan consists of both RFC and MRO NERC regions. Multiple TMY3 customers in utilities except in California line up and cannot be differentiated due to the scale of the plot.

An important observation in Figure 3.3 is that PG&E and SCE customers have significantly different CO_2 emissions impacts. SCE customers CO_2 increase the emissions in the winter months and reduces CO_2 emissions in the summer months. We observe the opposite effect from PG&E customers. This change in CO_2 emissions comes from the different timing of on-peak and off-peak periods in two utilities. During the summer period, SCE incentivizes its customers to discharge their ESS much earlier than PG&E. This two hours, in fact, have power generators at the margin that have high CO_2 emissions. On the contrary the generators for the same two hours in the winter period have lower CO_2 emissions than later in the night. Presumably both utility could trigger CO_2 emission reductions if SCE would shift the on-peak period pricing in winter forward and PG&E would shift the on-peak period pricing in summer backward.

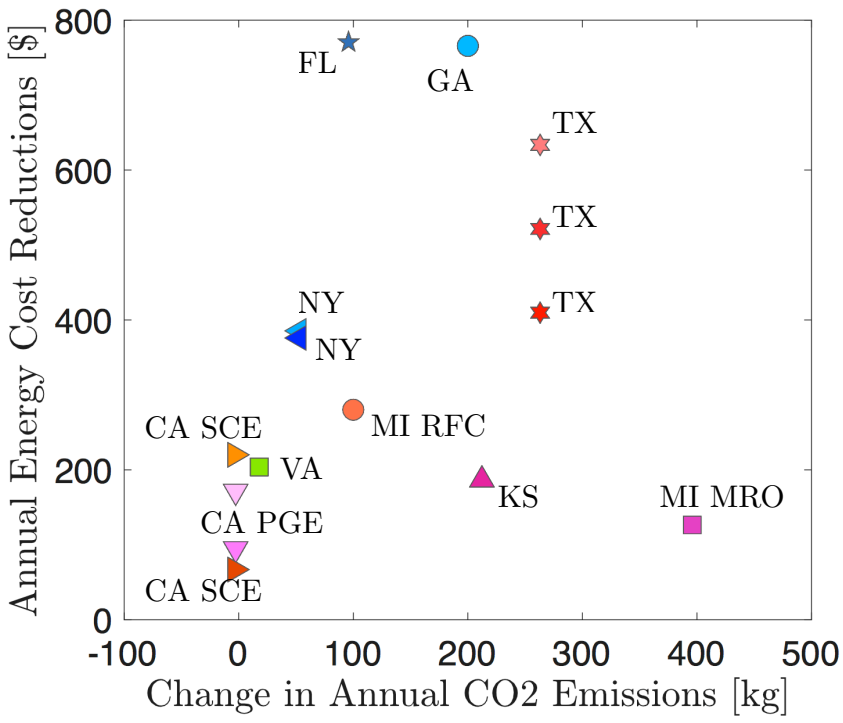

Figure 3.5. The change in annual CO_2 emission and the annual energy cost reductions averaged over all customers in each utility service area. (Customer #3, configuration *d*, that is, ESS + PV with net metering)

The overall results for the customer type #2 with configuration *a* are given in Figure 3.4. We observe that the trend for California where some customers could reduce emissions through ESS scheduling do not apply for the remainder of the states. The closest follower of California is Virginia with all customers analyzed cause an increase in CO_2 emissions. We see that some states (e.g. Florida, Georgia and Texas) do very well in terms of incentivizing the customers to adopt ESS with large annual energy cost reductions in their electricity bills. Michigan customers that are served within MRO region cannot reduce their electricity bills as much as customers in other states and have the highest impact on the CO_2 emissions.

The CO_2 emission results for the customer type #3 with configuration *c* are given in Figure 3.5. This case represents the customer with an ESS and a solar PV system under a net metering program. We observe that the variation between customers within the same utility is now disappeared. Since net metering is allowed, each ESS can now arbitrage between off-peak and on-peak periods and thereby operates independent of the load and solar profile of the customer. As a result, the resulting ESS schedules become completely dependent on the utility tariff structure as also observed in Section 2.2. The final conclusion is that under a net metering program adopting a solar PV system does not effectively increase the earnings of a customer coming from the ESS itself and does not alleviate the emissions impact of the ESS that we observed in the ESS only case.

Chapter 3, in part, is currently being prepared for submission for publication of material. Babacan, Oytun; Hanna, Ryan; Abdulla, Ahmed; Kleissl, Jan; Victor, David. The dissertation author is the primary investigator and author of this article.

Chapter 4

Concluding Remarks

In this dissertation we investigated how energy storage technologies could help the ongoing transformation of the electric grid. We described a bi-level optimization method in Chapter 1 that reduces the voltage fluctuations caused by PV penetration through deploying ESS in strategic nodes of distribution systems. We developed a convex optimization based ESS charge/discharge scheduling algorithm in Chapter 2 that minimizes the monthly electricity expenses of a customer. We also demonstrated that the novel idea of a "supply charge" tariff could incentivize ESS customers to store excess solar PV generation that may otherwise result in reverse power flow in the distribution grid. Finally, in Chapter 3, we explained the economic and emissions effects of residential energy storage operation for cost minimization service.

We have demonstrated how ESS technologies could provide benefits (1) to the electric grid through alleviating voltage fluctuations caused by solar PV generation, (2) to the customers through reducing their electricity bills while also providing ancillary services to the electric grid, and (3) to the environment through facilitating self-consumption of excess solar PV generation and reducing overall emissions of the electric power sector. It is our hope that the assessments presented in this dissertation would assist regulators and policy makers in their efforts to decarbonize and modernize the electric grid.

Bibliography

Alam, M. J. E., Muttaqi, K. M., Sutanto, D., jul 2012. Distributed energy storage for mitigation of voltage-rise impact caused by rooftop solar PV. In: 2012 IEEE Power and Energy Society General Meeting. Institute of Electrical and Electronics Engineers (IEEE).
URL http://dx.doi.org/10.1109/PESGM.2012.6345726

Arritt, R. F., Dugan, R. C., 2010. The IEEE 8500-node test feeder. In: IEEE PES T&D 2010. Institute of Electrical and Electronics Engineers (IEEE), pp. 1–6.
URL http://dx.doi.org/10.1109/TDC.2010.5484381

Atwa, Y. M., El-Saadany, E. F., nov 2010. Optimal allocation of ESS in distribution systems with a high penetration of wind energy. IEEE Transactions on Power Systems 25 (4), 1815–1822.
URL http://dx.doi.org/10.1109/TPWRS.2010.2045663

Ausgrid, 2016. Price lists and policy: Network price list 2016 - 2017. Online; accessed Feb. 2017.
URL http://www.ausgrid.com.au/Common/Industry/Regulation/Network-prices/Price-lists-and-policy.aspx

Back, T., 1 1996. Evolutionary Algorithms in Theory and Practice, 1st Edition. Evolution Strategies, Evolutionary Programming, Genetic Algorithms. Oxford University Press, New York, NY, USA.

Baran, M. E., El-Markabi, I. M., Jan. 2007. A Multiagent-Based Dispatching Scheme for Distributed Generators for Voltage Support on Distribution Feeders. IEEE Transactions on Power Systems 22 (1), 52–59.
URL http://dx.doi.org/10.1109/TPWRS.2006.889140

Baran, M. E., Hooshyar, H., Shen, Z., Huang, A., Jun. 2012. Accommodating high PV penetration on distribution feeders. IEEE Transactions on Smart Grid 3 (2), 1039–1046.
URL http://dx.doi.org/10.1109/TSG.2012.2190759

Bettle, R., Pout, C., Hitchin, E., dec 2006. Interactions between electricity-saving measures and carbon emissions from power generation in england and wales. Energy Policy 34 (18), 3434–3446.
URL https://doi.org/10.1016/j.enpol.2005.07.014

BNEF, 2017. New energy outlook 2016 powering a changing world. Tech. rep., Bloomberg New Energy Finance.

Borges, C. L. T., Falcão, D. M., Jul. 2006. Optimal distributed generation allocation for reliability, losses, and voltage improvement. International Journal of Electrical Power & Energy Systems 28 (6), 413–420.
URL http://dx.doi.org/10.1016/j.ijepes.2006.02.003

Carson, R. T., Novan, K., nov 2013. The private and social economics of bulk electricity storage. Journal of Environmental Economics and Management 66 (3), 404–423.
URL https://doi.org/10.1016/j.jeem.2013.06.002

Carvalho, P., Correia, P., Ferreira, L., may 2008. Distributed Reactive Power Generation Control for Voltage Rise Mitigation in Distribution Networks. IEEE Transactions on Power Systems 23 (2), 766–772.
URL http://dx.doi.org/10.1109/TPWRS.2008.919203

Celli, G., Ghiani, E., Mocci, S., Pilo, F., may 2005. A multiobjective evolutionary algorithm for the sizing and siting of distributed generation. IEEE Transactions on Power Systems 20 (2), 750–757.
URL http://dx.doi.org/10.1109/TPWRS.2005.846219

Celli, G., Mocci, S., Pilo, F., Loddo, M., jun 2009. Optimal integration of energy storage in distribution networks. In: 2009 IEEE Bucharest PowerTech. Institute of Electrical and Electronics Engineers (IEEE).
URL http://dx.doi.org/10.1109/PTC.2009.5282268

Chen, C., Duan, S., Cai, T., Liu, B., Hu, G., oct 2011. Optimal allocation and economic analysis of energy storage system in microgrids. IEEE Transactions on Power Electronics 26 (10), 2762–2773.
URL http://dx.doi.org/10.1109/TPEL.2011.2116808

Chiradeja, P., Ramakumar, R., Dec. 2004. An approach to quantify the technical benefits of distributed generation. IEEE Transactions on Energy Conversion 19 (4), 764–773.
URL http://dx.doi.org/10.1109/TEC.2004.827704

Cutter, E., Haley, B., Hargreaves, J., Williams, J., Jul. 2014. Utility scale energy storage

and the need for flexible capacity metrics. Applied Energy 124, 274–282.

de Sisternes, F. J., Jenkins, J. D., Botterud, A., Aug. 2016. The value of energy storage in decarbonizing the electricity sector. Applied Energy 175, 368–379.
URL https://doi.org/10.1016/2Fj.apenergy.2016.05.014

Denholm, P., Ela, E., Kirby, B., Milligan, M., Jan. 2010. The Role of Energy Storage with Renewable Electricity Generation. Tech. rep., National Renewable Energy Laboratory.
URL http://www.nrel.gov/docs/fy10osti/47187.pdf

DiOrio, N., Dobos, A., Janzou, S., Nov. 2015. Economic analysis case studies of battery energy storage with SAM. Tech. rep., National Renewable Energy Laboratory.
URL http://www.nrel.gov/docs/fy16osti/64987.pdf

Electric Power Research Institute, 2008. Open distribution system simulator (opendss) version 7.6.4.36. Http://smartgrid.epri.com/SimulationTool.aspx.

Geem, Z. W., Yoon, Y., Mar. 2017. Harmony search optimization of renewable energy charging with energy storage system. International Journal of Electrical Power & Energy Systems 86, 120–126.
URL https://doi.org/10.1016/2Fj.ijepes.2016.04.028

Gitizadeh, M., Fakharzadegan, H., Feb. 2014. Battery capacity determination with respect to optimized energy dispatch schedule in grid-connected photovoltaic (PV) systems. Energy 65, 665–674.
URL https://doi.org/10.1016/2Fj.energy.2013.12.018

GTM Research, ESA, 2017. U.S. energy storage monitor: 2016 year in review and Q1 2017. Tech. rep., GTM Research/ESA.

GTM Research, SEIA, 2015. U.s. solar market insight report q1 2015 executive summary. Tech. rep., GTM Research/SEIA.

Hanna, R., Kleissl, J., Nottrott, A., Ferry, M., may 2014. Energy dispatch schedule optimization for demand charge reduction using a photovoltaic-battery storage system with solar forecasting. Solar Energy 103, 269–287.
URL http://dx.doi.org/10.1016/j.solener.2014.02.020

Hawkes, A., oct 2010. Estimating marginal CO2 emissions rates for national electricity systems. Energy Policy 38 (10), 5977–5987.
URL https://doi.org/10.1016/j.enpol.2010.05.053

Hendron, R., Engebrecht, C., 2010. Building america house simulation protocols. Tech. rep., National Renewable Energy Laboratory.

Hittinger, E. S., Azevedo, I. M. L., mar 2015. Bulk energy storage increases united states electricity system emissions. Environmental Science & Technology 49 (5), 3203–3210.
URL https://doi.org/10.1021/es505027p

Hledik, R., Aug. 2014. Rediscovering residential demand charges. The Electricity Journal 27 (7), 82–96.
URL https://doi.org/10.1016/2Fj.tej.2014.07.003

Horn, J., Nafpliotis, N., Goldberg, D., 1994. A niched pareto genetic algorithm for multiobjective optimization. In: Proceedings of the First IEEE Conference on Evolutionary Computation. IEEE World Congress on Computational Intelligence. Vol. 1. Institute of Electrical and Electronics Engineers (IEEE), pp. 82–87.
URL http://dx.doi.org/10.1109/ICEC.1994.350037

IFC, 2017. Energy storage trends and opportunities in emerging markets. Tech. rep., International Finance Cooperation.

Jamaly, M., Bosch, J. L., Kleissl, J., apr 2013. Aggregate ramp rates of distributed photovoltaic systems in san diego county. IEEE Transactions on Sustainable Energy 4 (2), 519–526.
URL https://doi.org/10.1109/tste.2012.2201966

Jamasb, T., Pollitt, M. G., 2011. The Future of Electricity Demand: Customers, Citizens and Loads. Department of Applied Economics Occasional Papers. Cambridge University Press.

Kabiri, R., Holmes, D. G., McGrath, B. P., sep 2014. Voltage regulation of LV feeders with high penetration of PV distributed generation using electronic tap changing transformers. In: 2014 Australasian Universities Power Engineering Conference, AUPEC 2014 - Proceedings. Royal Melbourne Institute of Technology University, Melbourne, Australia, Institute of Electrical & Electronics Engineers (IEEE), pp. 1–6.
URL http://dx.doi.org/10.1109/AUPEC.2014.6966635

Luthander, R., Widén, J., Munkhammar, J., Lingfors, D., Oct. 2016. Self-consumption enhancement and peak shaving of residential photovoltaics using storage and curtailment. Energy 112, 221–231.
URL https://doi.org/10.1016/2Fj.energy.2016.06.039

Marnay, C., Fisher, D., Murtishaw, S., Phadke, A., Price, L., Sathaye, J., 2002. Estimating

carbon dioxide emissions factors for the california electric power sector. Tech. rep., Lawrence Berkeley National Laboratory.

McLaren, J., Davidson, C., Miller, J., Bird, L., Oct. 2015. Impact of rate design alternatives on residential solar customer bills: Increased fixed charges, minimum bills and demand-based rates. The Electricity Journal 28 (8), 43–58.

Mitchell, M., 1998. An Introduction to Genetic Algorithms. MIT Press, Cambridge, MA, USA.

Moradi, M., Abedini, M., jan 2012. A combination of genetic algorithm and particle swarm optimization for optimal DG location and sizing in distribution systems. International Journal of Electrical Power & Energy Systems 34 (1), 66–74.
URL http://dx.doi.org/10.1016/j.ijepes.2011.08.023

Moradi, M. H., Abedini, M., Hosseinian, S. M., nov 2015. Improving operation constraints of microgrid using PHEVs and renewable energy sources. Renewable Energy 83, 543–552.
URL http://dx.doi.org/10.1016/j.renene.2015.04.064

Morvaj, B., Evins, R., Carmeliet, J., jun 2016. Optimization framework for distributed energy systems with integrated electrical grid constraints. Applied Energy 171, 296–313.
URL http://dx.doi.org/10.1016/j.apenergy.2016.03.090

Moshövel, J., Kairies, K.-P., Magnor, D., Leuthold, M., Bost, M., Gährs, S., Szczechowicz, E., Cramer, M., Sauer, D. U., Jan. 2015. Analysis of the maximal possible grid relief from PV-peak-power impacts by using storage systems for increased self-consumption. Applied Energy 137, 567–575.
URL https://doi.org/10.1016/2Fj.apenergy.2014.07.021

National Solar Radiation Data Base, 2015. 1991- 2005 update: Typical meteorological year 3. Http://rredc.nrel.gov/solar/.

Neeland, H., sep 2009. The residential demand for electricity in the united states. Economic Analysis and Policy 39 (2), 193–203.
URL https://doi.org/10.1016/s0313-5926(09)50017-3

Nick, M., Cherkaoui, R., Paolone, M., sep 2014. Optimal allocation of dispersed energy storage systems in active distribution networks for energy balance and grid support. IEEE Trans. Power Syst. 29 (5), 2300–2310.
URL http://dx.doi.org/10.1109/TPWRS.2014.2302020

Open Energy Information, 2014. Commercial and residential hourly load profiles for all tmy3 locations in the united states. Http://en.openei.org.

Ranaweera, I., Midtgård, O.-M., Apr. 2016. Optimization of operational cost for a grid-supporting PV system with battery storage. Renewable Energy 88, 262–272.
URL https://doi.org/10.1016/2Fj.renene.2015.11.044

Ratnam, E. L., Weller, S. R., Kellett, C. M., Mar. 2015a. An optimization-based approach to scheduling residential battery storage with solar PV: Assessing customer benefit. Renewable Energy 75, 123–134.
URL https://doi.org/10.1016/2Fj.renene.2014.09.008

Ratnam, E. L., Weller, S. R., Kellett, C. M., Murray, A. T., Oct. 2015b. Residential load and rooftop PV generation: an Australian distribution network dataset. International Journal of Sustainable Energy, 1–20.
URL https://doi.org/10.1080/2F14786451.2015.1100196

Ren, H., Wu, Q., Gao, W., Zhou, W., Oct. 2016a. Optimal operation of a grid-connected hybrid PV/fuel cell/battery energy system for residential applications. Energy 113, 702–712.
URL https://doi.org/10.1016/2Fj.energy.2016.07.091

Ren, Z., Grozev, G., Higgins, A., Apr. 2016b. Modelling impact of PV battery systems on energy consumption and bill savings of Australian houses under alternative tariff structures. Renewable Energy 89, 317–330.
URL https://doi.org/10.1016/2Fj.renene.2015.12.021

REN21, 3 2015. Renewables 2015 global status report. Tech. rep., REN21.

Rothlauf, F., 2006. Representations for Genetic and Evolutionary Algorithms, 2nd Edition. Springer-Verlag Berlin, Heidelberg.
URL http://dx.doi.org/10.1007/3-540-32444-5

Siler-Evans, K., Azevedo, I. L., Morgan, M. G., may 2012. Marginal emissions factors for the u.s. electricity system. Environmental Science & Technology 46 (9), 4742–4748.
URL https://doi.org/10.1021/es300145v

Srinivas, N., Deb, K., sep 1994. Muiltiobjective optimization using nondominated sorting in genetic algorithms. Evolutionary Computation 2 (3), 221–248.
URL http://dx.doi.org/10.1162/evco.1994.2.3.221

U.S. Energy Information Administration, 2016. Electric power sales, revenue, and energy

efficiency form eia-861 detailed data files. Http://rredc.nrel.gov/solar/.

Vieira, F. M., Moura, P. S., de Almeida, A. T., Apr. 2017. Energy storage system for self-consumption of photovoltaic energy in residential zero energy buildings. Renewable Energy 103, 308–320.
URL https://doi.org/10.1016/2Fj.renene.2016.11.048

Voorspools, K. R., D'haeseleer, W. D., nov 2000. An evaluation method for calculating the emission responsibility of specific electric applications. Energy Policy 28 (13), 967–980.
URL https://doi.org/10.1016/s0301-4215(00)00080-x

Vose, M. D., 1999. The Simple Genetic Algorithm: Foundations and Theory. MIT Press, Cambridge, MA, USA.

Wilcox, S., Marion, W., 2008. Users manual for tmy3 data sets. Tech. rep., National Renewable Energy Laboratory.

Zhang, Y., Lundblad, A., Campana, P. E., Yan, J., Jun. 2016. Employing battery storage to increase photovoltaic self-sufficiency in a residential building of Sweden. Energy Procedia 88, 455–461.
URL https://doi.org/10.1016/2Fj.egypro.2016.06.025

Zheng, M., Meinrenken, C. J., Lackner, K. S., Jun. 2015. Smart households: Dispatch strategies and economic analysis of distributed energy storage for residential peak shaving. Applied Energy 147, 246–257.
URL https://doi.org/10.1016/2Fj.apenergy.2015.02.039